



Effects of 21st century climate change on seasonal flow regimes and hydrologic extremes over the Midwest and Great Lakes region of the US

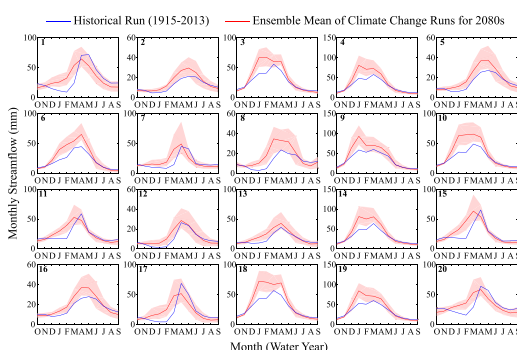
Kyuhyun Byun ^{*}, Chun-Mei Chiu, Alan F. Hamlet

Department of Civil and Environmental Engineering and Earth Sciences, College of Engineering, University of Notre Dame, Notre Dame, IN 46556, United States of America

HIGHLIGHTS

- By the 2080s, the simulated 100-yr flood increases in most Midwestern rivers.
- The timing of monthly mean and annual peak flows is projected to shift earlier.
- Extreme low soil moisture and extreme low flows decline by the 2080s.
- Changes in extremes are attributable to shifts in several hydrologic variables.

GRAPHICAL ABSTRACT



ARTICLE INFO

Article history:

Received 5 July 2018

Received in revised form 2 September 2018

Accepted 5 September 2018

Available online 7 September 2018

Editor: Wei Ouyang

Keywords:

Climate change

Hydrologic extremes

Midwest and Great Lakes

Flooding

Low flows

Extreme low soil moisture

ABSTRACT

Analyzing future changes in hydrologic extremes such as floods, low flows, and soil moisture extremes is important because many impacts on ecosystems and human systems occur during extreme events. To quantify changes in hydrologic extremes, this study conducts hydrologic modeling experiments over 20 Midwestern watersheds using the Variable Infiltration Capacity (VIC) model forced by historical observed datasets and future projections from statistically downscaled Global Climate Model (GCMs) simulations. Our results show that peak daily streamflow at the 100-yr recurrence interval will increase (+10–30%) in most watersheds by 2080s due to significant increases in precipitation (P) and increasing P as rainfall during winter and spring seasons. The simulations also show strong shifts towards earlier peak flow timing (up to a month), especially in strongly snowmelt-dominated watersheds. These effects are linked to strong decreasing trends in maximum Snow Water Equivalent (SWE) with warming, which are simulated over essentially the entire domain. Projected changes in 7-day extreme low flows are smaller in magnitude (−10–+10%) with somewhat larger decreases simulated at the end of century; however, the timing of extreme low flows is projected to shift from winter/spring to summer and fall in strongly snowmelt-dominated watersheds in the northernmost parts of the domain. Extreme low soil moisture increases over most of the domain in the future projections up to the 2050s, but by the 2080s there are more widespread decreases in extreme low soil moisture, especially in the northernmost parts of the domain.

© 2018 Elsevier B.V. All rights reserved.

1. Introduction

There is a steadily increasing body of evidence supporting the conclusion that climate change will have critical impacts on both natural ecosystems and human society (Doney et al., 2012; IPCC, 2013; Kumar

^{*} Corresponding author.

E-mail address: kbyun@nd.edu (K. Byun).

and Lawrence, 2014; Parmesan and Yohe, 2003; Patz et al., 2005; Wheeler and von Braun, 2013). In particular, changing hydrometeorological extremes under climate change are expected to affect regional ecosystems and human communities via impacts on water supply, agriculture, hydropower production, flooding, low flows, stormwater infrastructure, and aquatic and terrestrial ecosystems (Howden et al., 2007; Knapp et al., 2008; Parsons et al., 2005; Rosenberg et al., 2010; Schewe et al., 2014; Vörösmarty et al., 2000; Wenger et al., 2011; Zhou et al., 2012). However, hydrologic response to climate change is also known to be regionally specific due to baseline climate, specific storm characteristics (e.g. presence or absence of hurricanes and atmospheric rivers), and differences in surface and subsurface features (e.g. characteristics associated with topography, vegetation, subsurface geology, etc.) (Fischer et al., 2007; Hay et al., 2011). Thus, in order to understand the potentially changing behavior of hydrologic systems and to support the development of effective and sustainable climate change adaptation strategies, detailed hydrologic modeling of extremes at the river basin scale is required to quantify impacts in specific regions and watersheds. Such studies also motivate climate change mitigation efforts at the regional, national, and global scale.

A number of existing regional-scale studies have shown that hydrologic extremes will be significantly changed by an altered climate (Madsen et al., 2014; Milly et al., 2002, 2008; Sheffield and Wood, 2008; Tohver et al., 2014; Touma et al., 2015), but any general conclusions (e.g. at the scale of the entire U.S.) cannot be made due to regionally specific changes in temperature and precipitation forcings, varying hydrologic mechanisms that inform local flood responses, and human activities (Haddeland et al., 2014; Hirsch and Ryberg, 2012). Existing studies in the U.S. have focused primarily (though not exclusively) on the western U.S. and mountain watersheds where loss of snowpack has been an important factor (Barnett et al., 2008; Cayan et al., 2010; Hamlet et al., 2013; Kim, 2005; Rasmussen et al., 2014; Tohver et al., 2014). A smaller number of studies (Cherkauer and Sinha, 2010; Demaria et al., 2016; Naz et al., 2016) have investigated the effects of climate change on hydrologic extremes in the Midwest and Great Lakes region. The topography in the Midwest is much less complex, but the underlying climatology that defines hydrologic extremes is associated with extreme seasonal temperature range, small-scale convective storms in warm season, and large-scale cyclonic storms in winter. The Midwest's historical climate (and response to climate change) is also substantially impacted by the presence of the Great Lakes (Sharma et al., 2018).

During the past decade there have been an increasing number of studies showing that regional climate will likely be significantly altered in the late 21st century over the Midwest and Great Lakes region (e.g. Byun and Hamlet, 2018; Hayhoe et al., 2010; Pryor et al., 2014). Although there are some differences between these studies, all showed substantial warming trends for the future, and projected wetter conditions in cool season and drier conditions in warm season by the end of the 21st century.

The hydrologic effects of projected climate change over the Midwest and Great Lakes region remains an important concern for long-term planning and climate change adaptation, and modeling future hydrologic extremes is particularly challenging because of the non-linear behavior of hydrologic systems and complex sensitivity to climate variability and change. A few recent case studies at the watershed scale (e.g. Chien et al., 2013; Li et al., 2016; Verma et al., 2015) have pointed out some key challenges in analyzing future hydrologic impacts at watershed scale. For example, obtaining fine-scale climate data through statistical or dynamic downscaling of GCMs requires extensive computational resources and is practically complex (Hamlet et al., 2013; Wang et al., 2015). Li et al. (2016) point out that uncertainty quantification is extremely challenging because there are multiple uncertainty sources in the analysis. Among these are a range of future climate projections from different GCMs, selection of GCM ensembles (Chen et al., 2011), choice of downscaling method, and sensitivity of hydrologic models to climate forcing (Hattermann et al., 2017).

Several past studies have examined the changing nature of hydro-meteorological extremes for a few specific watersheds or several groups of basins in the Midwest. For example, Cherkauer and Sinha (2010) analyzed future hydrologic extremes using a previous version (Coupled Model Intercomparison Project Phase 3, CMIP3) of GCMs over 6 major basins surrounding Lake Michigan. In a more recent study, Demaria et al. (2016) showed projected changes in peak and low extreme streamflow based on the projections at relatively coarse resolution (1/8°) produced by a simple downscaling approach. The results were also represented mostly as three big groups of the Midwest region. These studies all demonstrated that there will likely be significant impacts on hydrologic extremes over the Midwest by the end of the 21st century. However, a more detailed and complete analysis is needed to extend these initial findings over an important but relatively understudied region. In particular there is a need to (1) carry out intensive analysis on a larger number of watersheds to better characterize variations in hydrologic response to changing climate, (2) use the most recent climate data from the Coupled Model Intercomparison Project, phase 5 (CMIP5), (3) use a well-validated statistical downscaling approach for hydrologic projection at finer resolution than previous studies, and (4) extend hydrologic extremes analysis to include additional variables such as snowpack and soil moisture, and address other important characteristics of future extremes such as the seasonal timing of extreme high and low streamflow events.

Specifically, this study will address some important scientific questions in this region: (1) What is the historical timing of “regime shifts” (i.e. systematic shifts in mean values associated with decadal-scale climate variability) in annual peak flows for different watersheds? Are there similarities between different watersheds identified by this analysis? (2) How will climate change alter the magnitude and timing of hydro-meteorological extremes in specific watersheds? (3) Can we attribute projected changes in extremes to physical watershed characteristics or specific hydrological responses under changing climate over this region? For example, will antecedent hydrologic conditions such as snowpack or soil moisture be an important factor affecting hydro-meteorological extremes in the future, or will the changing nature of extreme storms (e.g. seasonal timing of changing precipitation type and intensity) be a more dominant factor?

The purpose of this study is to answer the aforementioned questions by projecting and analyzing the changing magnitude and timing of hydrologic extremes for 20 watersheds in the Midwest and Great Lakes region in response to a) changing observed conditions in long historical records and b) an ensemble of regional climate change projections from the CMIP5. For historical conditions we use both USGS observations and hydrologic model simulations to analyze changing conditions. For future conditions we analyze changing hydrologic extremes by one-way coupling (linking) a series of numerical models. Statistically-downscaled future projections of temperature (P) and precipitation (P) from a group of 6 GCMs (Byun and Hamlet, 2018) are used as inputs to a macro-scale hydrologic model which simulates hydrological variables such as runoff, baseflow, snow water equivalent (SWE) and soil moisture (SM) at daily time step. Combined runoff and baseflow are then used as inputs to a daily-time-step routing model to simulate changes in daily and monthly streamflow statistics, and estimate high- and low-flow extremes.

2. Data sources and methods

2.1. Study area

Our domain for the study is the Midwest and Great Lakes region covering the Great Lakes drainages in the U.S. and nine states touching these watershed boundaries: Illinois, Indiana, Iowa, Michigan, Minnesota, New York, Ohio, Pennsylvania, and Wisconsin. Fig. 1 shows this domain and major land cover types from remotely sensed data. Within this domain we selected 20 watersheds from the Hydro-Climatic Data

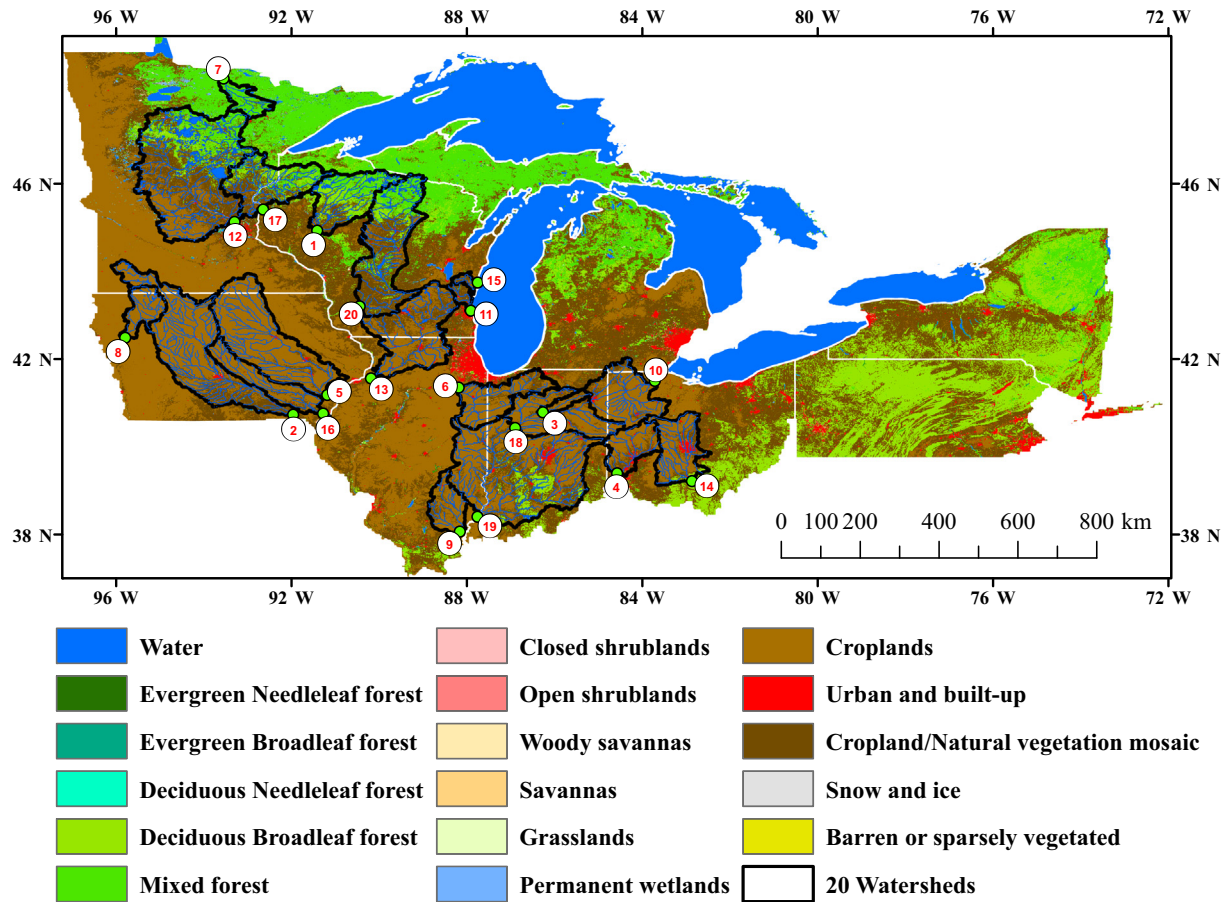


Fig. 1. Study domain and 20 HCDN watersheds in the Midwest and Great Lakes region shown with remotely sensed land cover provided by MODIS at 500 m resolution. Our hydrologic simulations are processed at 1/16° resolution within this domain.

Network (HCDN) defined by U.S. Geological Survey (USGS) (Slack and Landwehr, 1992). Observed streamflow data archived at HCDN sites are relatively free of anthropogenic influences such as diversions and reservoirs and thus can be readily compared with hydrologic model simulations of natural conditions. More detailed information on the gage stations for the 20 watersheds including location, temporal coverage and contributing basin area can be found in Table 1.

In selecting the 20 watersheds in this study (please also see Section 2.4.2 Evaluation of streamflow simulations), we first validated our hydrologic model over a larger group of 40 HCDN watersheds, and then selected a subset of 20 watersheds where our hydrologic model shows reasonable performance for reproducing both observed monthly and annual maximum daily streamflow (see Table S1). Also, we considered the spatial distribution of 20 watersheds to account for the variability of hydrologic conditions over the domain.

Table 1

The information on 20 watersheds and its USGS streamflow gauge station in HCDN.

#No	Watershed	Gauge location	Drainage area (km ²)	Temporal coverage
1	Chippewa	USGS 05365500 at Chippewa Falls, WI	14,633.4	Jun. 1888 -
2	Des Moines	USGS 05490500 at Keosauqua, IA	36,358.3	May 1903 -
3	EEL	USGS 03328500 near Logansport, IN	2043.5	Oct. 1943 -
4	Great Miami	USGS 03274000 at Hamilton, OH	9401.7	Apr. 1927 -
5	Iowa	USGS 05465500 at Wapello, IA	32,374.9	Oct. 1914 -
6	Kankakee	USGS 05527500 near Wilmington, IL	13,338.4	Nov. 1914 -
7	Little Fork	USGS 05131500 at Littlefork, MN	4351.2	Jul. 1909 -
8	Little Sioux	USGS 06606600 at Correctionville, IA	6475.0	May 1918 -
9	Little Wabash	USGS 03381500 at Carmi, IL	8034.1	Oct. 1939 -
10	Maumee	USGS 04193500 at Waterville, OH	16,394.6	Nov. 1898 -
11	Milwaukee	USGS 04087000 at Milwaukee, WI	1802.6	Apr. 1914 -
12	Mississippi	USGS 05288500 at Brooklyn, Park, MN	49,468.8	Jun. 1931 -
13	Rock	USGS 05446500 near Joslin, IL	24,731.8	Oct. 1939 -
14	Scioto	USGS 03234500 at Higby, OH	13,289.2	Oct. 1930 -
15	Sheboygan	USGS 04086000 at Sheboygan, WI	1082.6	Jun. 1916 -
16	Skunk	USGS 05474000 at Augusta, IA	11,168.0	Sep. 1913 -
17	St. Croix	USGS 05340500 at St. Croix Falls, WI	16,161.5	Jan. 1902 -
18	M-Wabash	USGS 03335500 at Lafayette, IN	18,821.5	Oct. 1923 -
19	Wabash	USGS 03377500 at MT. Carmel, IL	74,164.4	Oct. 1927 -
20	Wisconsin	USGS 05407000 at Muscoda, WI	26,935.9	Oct. 1913 -

2.2. Gridded historical meteorological data set (1915–2013)

Historical meteorological data (Precipitation, Tmax, Tmin, and Wind Speed) for the study are provided by a gridded product from 1915 to 2013 at 1/16° latitude/longitude resolution ($\sim 5 \times 7$ km) based on interpolated station data (Chiu et al., personal communication). This product also includes precipitation gauge undercatch corrections using interpolated wind speed data from National Center for Atmospheric Research (NCAR) Reanalysis simulations (Kalnay et al., 1996). There are currently three versions of this meteorological data set a) V0, which is raw interpolated station data with no undercatch corrections, b) V1, which applies uniform corrections to rain and snow in all areas of the domain, and c) V2, which makes uniform corrections for rain, but different snow corrections in different parts of the domain based on estimates of the rain/snow ratio established using a group of high-quality station records. In this study we make use of the V1 data set and downscaled climate products based on these data (see Byun and Hamlet (2018) for additional details).

2.3. Future climate change projections

In order to simulate hydrologic conditions over the Midwest and Great Lakes region for future periods, we make use of statistically downscaled GCM projections prepared using the Hybrid Delta (HD) downscaling approach (Byun and Hamlet, 2018; Hamlet et al., 2013; Tohver et al., 2014). As its name suggests, the HD is a hybrid method that combines many advantages of both the classic Delta Method (DM) and the well-known Bias Correction and Spatial Disaggregation (BCSD) downscaling approach (Wood et al., 2004). For example, the daily time series behavior in the HD is based on the long-term variability from our historical datasets, while the monthly Cumulative Distribution Functions (CDFs) for each grid cell are forced to match those from GCM data downscaled by BCSD. A key advantage of the HD is that it preserves the large sample size of the historical meteorological data for each defined future period. This is an important advantage for analysis of hydrologic extremes in particular, because the analysis is based on a relatively large, common sample size for both historical and future periods. Thus estimates of extremes with high return intervals (e.g. the 100-year flood) can be made with greater confidence in comparison with other downscaling methods that typically use data from 30-year periods to estimate extremes (Byun and Hamlet, 2018; Hamlet et al., 2013; Tohver et al., 2014).

Future projections used in this study are based on two greenhouse gas concentration scenarios: Representative Concentration Pathways (RCP) 4.5 and 8.5, a medium and high scenario, respectively (van Vuuren et al., 2011). Results for three future periods keyed to 30-year windows centered on 2020s (2011–2040), 2050s (2041–2070) and 2080s (2071–2100) are archived for six different GCMs (Table 2) which a) well reproduce Midwest climate variability, and b) span the range of T and P changes projected by 31 GCMs over the Midwest region (Byun and Hamlet, 2018). Note that although the results are keyed to 30-yr time windows in the future (which determine the monthly CDFs), all 36 future data sets (i.e. $2 \times 3 \times 6$) have the same sample

size and basic time series as the 1915–2013 historical meteorological data set described above. More details on retrospective performance of GCMs over the Midwest, changes in T and P predicted by different GCMs, and the HD downscaling process are given by Byun and Hamlet (2018).

2.4. Macro-scale hydrologic model

For hydrologic model experiments in the study area, we use the physically based Variable Infiltration Capacity (VIC) macro-scale hydrologic model (Liang et al., 1994, 1996). The mostly physically based VIC model, which takes into account sub-grid variability in vegetation and topography, has been widely used in climate change impact assessment studies (Hamlet et al., 2013; Livneh et al., 2013; Vano et al., 2015; Wong et al., 2015). We implement the VIC model (version 4.1.2) over the domain shown in Fig. 1 at high spatial resolution (1/16°) with initial vegetation and soil parameters provided by Livneh et al. (2013). The model is run in water balance mode at 1-hour time step when snow is present, and at daily time step otherwise. Daily runoff and baseflow simulations for each cell are then routed using a simple streamflow routing model based on simple block unit hydrographs for each 1/16° cell, a flow direction file representing the routing network, and estimates of travel time from the cell to the outlet point (Lohmann et al., 1998). A new routing network and flow direction file for the Midwest and Great Lakes Region at 1/16° degree resolution was created and validated for this study (See Acknowledgements).

2.4.1. Overview of VIC model simulations

A single baseline historical run (HR) of the VIC model was made using the gridded meteorological dataset (1915–2013) as forcing. Removing the first nine months of the simulation for model spin up results in 98 water years of simulated daily data (1916–2013). For the future analysis, we force the VIC model with 36 unique HD data sets described above, which hereafter are referred to as Climate Change Runs (CCRs). Each CCR also has 98 years of daily data with essentially the same time series behavior as the historical observations, but different monthly statistics for T and P deriving from the downscaled GCM simulations.

2.4.2. Evaluation of streamflow simulations

Several past studies (Mendoza et al., 2015; Tohver et al., 2014) have demonstrated that the effect of detailed hydrologic model calibration on the ratio of future to historical flood simulations is relatively small, but hydrologic simulations should nonetheless capture the variability of observed streamflow reasonably well. To avoid the difficult and time-consuming process of calibrating the VIC model over a large number of watersheds, we took the alternate approach of selecting a group of 20 watersheds for which the existing VIC model calibration was acceptable. Reducing the number of streamflow locations also reduced the need for computational resources and made the presentation of results more tractable. We validated the model's performance for a larger group of 40 HCDN watersheds and then selected a smaller group of 20 watersheds with acceptable validation statistics (Table S1). Specifically,

Table 2
List of CMIP5 GCMs selected for VIC simulation.

No.	Model	Institute	Spatial resolution (latitude° × longitude°)	Emission scenarios
1	CESM1-CAM5	National Center for Atmospheric Research, USA	0.94 × 1.25°	RCP4.5/RCP8.5
2	FIO-ESM	The First Institute of Oceanography, SOA, China	2.81 × 2.79°	RCP4.5/RCP8.5
3	GFDL-CM3	Geophysical Fluid Dynamics Laboratory, NOAA, USA	2.0 × 2.5°	RCP4.5/RCP8.5
4	GFDL-ESM2M	Geophysical Fluid Dynamics Laboratory, NOAA, USA	2.0 × 2.5°	RCP4.5/RCP8.5
5	HadGEM2-AO	National Institute of Meteorological Research, Korea Meteorological Administration, South Korea	1.25 × 1.88°	RCP4.5/RCP8.5
6	HadGEM2-CC	Met Office Hadley Centre, UK	1.25 × 1.88°	RCP4.5/RCP8.5

we selected a group of 20 watersheds for which validation results (Figs. 2 and 3 and Table 3) showed good performance of the VIC model in reproducing observed seasonal and annual extreme streamflow. The most important aspect of the modeling in the context of this study is the sensitivity to changing climate, rather than the model's fidelity in reproducing observations. Additional calibration might improve the latter to some extent, but we argue has relatively little effect on the former (Mendoza et al., 2015; Tohver et al., 2014). This informs our choice not to invest resources in detailed calibration here, and instead we focus on the change of hydrologic variables (e.g. the ratio of the future 100-year flood magnitude to historical 100-year flood magnitude) rather than presenting absolute values of these variables. In order to evaluate the model's performance in reproducing observed monthly and daily peak streamflow, we calculate some basic statistics including correlation coefficient (r), bias, and root mean squared error (RMSE) (Table 3). Mathematical details of this statistical analysis are provided below.

2.5. Statistical tools for model evaluation and metrics for hydrologic change

In order to evaluate the VIC model's performance in reproducing observed monthly and daily peak streamflow, we calculate some basic statistics including correlation coefficient (r), bias, and root mean squared error (RMSE) as follows:

$$r = \frac{n(\sum S \cdot O) - (\sum S)(\sum O)}{\sqrt{[n \sum S^2 - (\sum S)^2]} \sqrt{[n \sum O^2 - (\sum O)^2]}} \quad (1)$$

$$BIAS = \frac{1}{n} \sum (S - O) \quad (2)$$

$$RMSE = \sqrt{\frac{1}{n} \sum (S - O)^2} \quad (3)$$

where S and O represent the simulated and observed streamflow, respectively, at each time step, and n is the number of samples.

In this study, a change in the magnitude and frequency of extreme events is evaluated by individually fitting the Generalized Extreme Value (GEV) distribution to each simulated data set of the annual daily extremes. The GEV distribution has been widely used for characterizing the statistical behavior of extreme values in climate change impact analysis (see e.g. Bennett et al., 2015; Tohver et al., 2014). The most general form of the GEV is based on three parameters: location (ξ), scale (α) and shape (κ), and the family of distributions encompasses several well-known extreme value distributions as special cases. The PDF of the Gumbel (aka Extreme Value Type I) distribution, for example, depends only on the location and scale parameters, with the shape parameter set to zero. A particular quantile from a GEV distribution associated with a given percentile can be calculated using the following formulas (Hosking and Wallis, 2005):

$$x_p = \xi + \frac{\kappa}{\alpha} [1 - (-\ln(P))^\kappa] \quad \kappa \neq 0 \quad (4a)$$

$$x_p = \xi - \alpha \ln(-\ln(P)) \quad \kappa = 0 \quad (4b)$$

where P is percentile and x_p is the extreme value associated with P (Note that Eq. 4b gives the quantile for the Gumbel distribution). For estimating of the parameters of the GEV distribution, we use L moment estimators based on probability weighted moments (Hosking et al., 1985; Hosking and Wallis, 2005).

In order to analyze the long-term trends in observed peak daily streamflow from USGS gage stations, we calculate the cumulative deviation from the mean (CDM) of peak daily streamflow for each water year from USGS observations as following:

$$CDM_k = \sum_{i=1}^k (X_i - \bar{X}) \quad k = 1, \dots, n \quad (5)$$

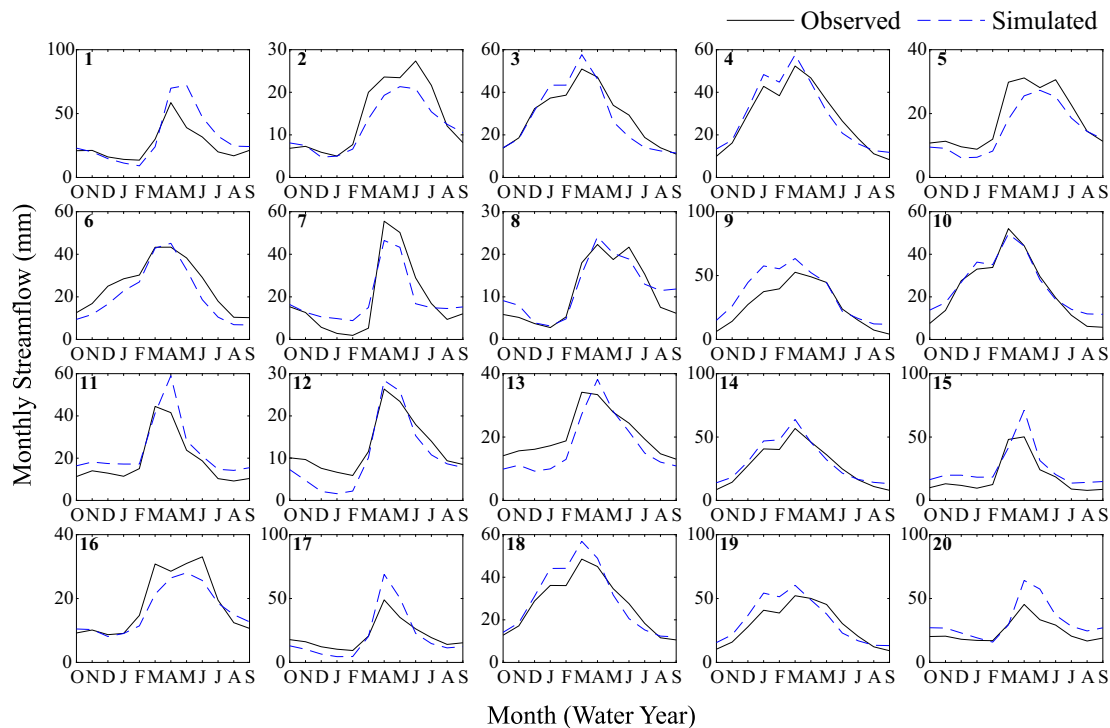


Fig. 2. Monthly streamflow at the outlets of each watershed by observed (black solid line) and historical run (HR, blue dotted line) of hydrologic simulation. Each panel represents the result for each watershed and the number in upper left corner matches to watershed ID number in Fig. 1 and Table 1.

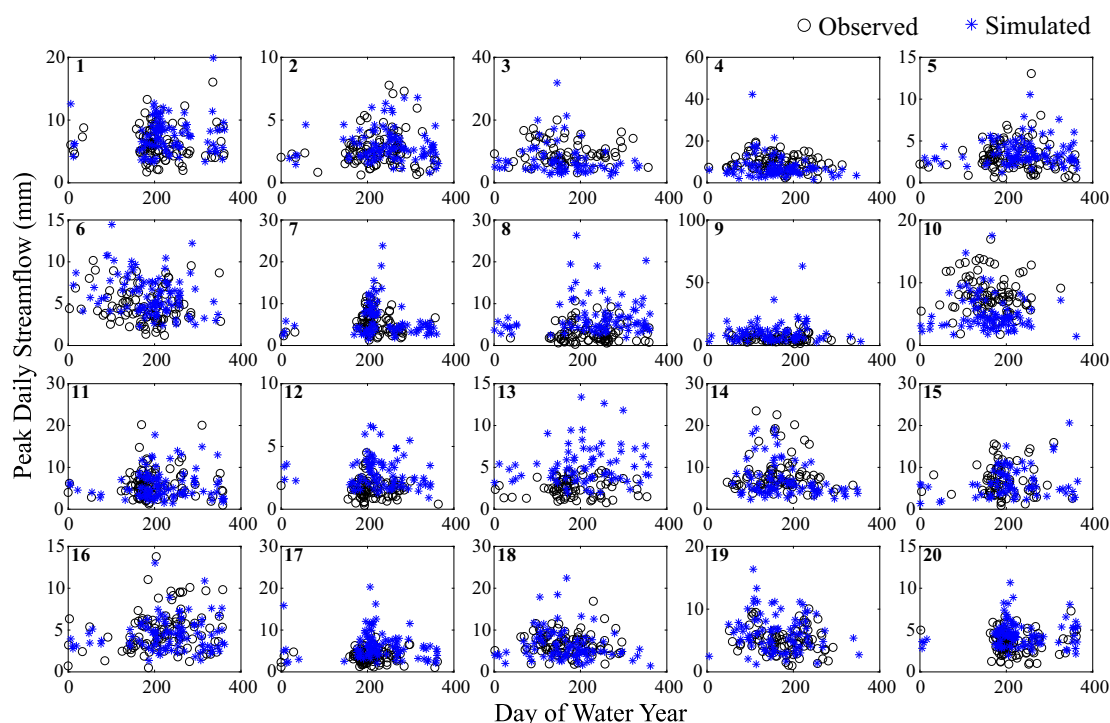


Fig. 3. Timing (DOY, x-axis) and magnitude (mm, y-axis) of peak daily streamflow for each water year at the outlets of each watershed; observed (black circle) and historical run (HR, blue asterisk). Each panel represents the result for each watershed and the number in upper left corner matches to watershed ID number in Fig. 1 and Table 1.

where X_i is the observed peak daily streamflow for i^{th} water year among available water year records (n), and \bar{X} is the mean of a series of X_i . The CDM analysis is intended to capture changes in extreme streamflow in response to decadal scale climate variability or other factors and is commonly used to identify “break points” in time where there is a characteristic shift from positive to negative anomalies (or vice versa). CDM ends with a value of zero by construction.

We assess changes in several hydrologic variables including peak daily streamflow and 7-day average extreme low streamflow, peak snow water equivalent (SWE), and extreme low total column soil moisture (SM) derived from HR and CCRs using the VIC model. For the representation of changes, we use percent change $(100 \cdot (V_{CCR} - V_{HR})/(V_{HR}))$.

More details on each variable are as followings:

- 1) To evaluate simulated flood risks, peak daily streamflow values during a water year (from October to September) were extracted and evaluated in terms of their magnitude and timing given by Day of Year (DOY, water year order). GEV parameters are then fitted to these annual extrema in order to compare peak flow events with a 100-year return interval for historical and future conditions.
- 2) 7Q10 low flow extremes were calculated based on simulated 7-day average daily low-flow extremes. The average of 7 consecutive day streamflow was calculated using a moving window, and the lowest 7-day average value during a water year were extracted. Parameters for the GEV distribution were then fitted to these low-flow extrema.

Table 3

Validation of the VIC model for monthly streamflow and peak daily streamflow. Watershed numbers match to those presented in Fig. 1 and Table 1.

#Watershed	Monthly streamflow				Peak daily streamflow			
	Correlation coefficient	Observed mean (mm)	Bias (mm)	RMSE (mm)	Correlation coefficient	Observed mean (mm)	Bias (mm)	RMSE (mm)
1	0.765	25.278	5.752	18.748	0.699	6.279	1.303	2.445
2	0.890	14.091	−1.948	8.303	0.681	2.655	0.325	1.093
3	0.867	28.777	−0.697	13.579	0.785	9.442	−1.996	3.721
4	0.919	28.016	1.135	11.370	0.636	9.482	−2.029	4.622
5	0.888	18.398	−3.333	9.337	0.825	3.151	0.478	1.160
6	0.897	25.501	−4.542	10.630	0.750	4.767	1.281	2.027
7	0.785	18.056	0.663	14.941	0.691	5.605	0.446	2.876
8	0.816	11.054	0.938	9.346	0.687	2.902	3.871	5.006
9	0.926	26.748	8.312	15.982	0.796	5.498	5.098	8.270
10	0.895	23.659	1.953	11.791	0.821	7.995	−2.993	3.425
11	0.843	18.598	4.772	13.556	0.595	5.827	−0.103	3.033
12	0.870	12.587	−2.194	6.829	0.760	1.605	1.315	1.550
13	0.855	20.712	−3.548	9.463	0.655	2.537	2.739	3.293
14	0.930	27.479	2.909	10.880	0.671	8.114	−1.160	3.570
15	0.867	18.601	6.381	15.256	0.655	6.742	−0.206	3.059
16	0.875	18.151	−1.730	11.405	0.783	4.858	−0.324	1.573
17	0.867	20.487	−0.512	15.303	0.781	3.687	2.702	3.507
18	0.915	27.245	1.870	11.082	0.641	6.536	−0.228	2.836
19	0.935	29.426	3.322	10.949	0.872	4.869	1.323	2.013
20	0.835	23.954	7.723	14.148	0.599	3.433	1.098	1.673

Then, 7-day low streamflow were evaluated in terms of 10-yr return interval (i.e. 7Q10), which corresponds to the 10th percentile (i.e. the probability of exceedance of 0.9) in the fitted GEV distribution.

- 3) We evaluated the maximum SWE during a water year (maximum accumulated snowpack on the land surface throughout a water year), focusing on changes in magnitude and timing (DOY) in order to evaluate the linkages between changes in peak daily streamflow and maximum SWE.
- 4) This study also analyzed extreme low SM (i.e. the lowest simulated total column soil moisture in each water year) across the region. In a similar manner to 7Q10 described above, 7-day extreme low values of total column SM (i.e. the sum of moisture from all three soil layers) in each grid cell were evaluated for the HR and CCRs.

3. Results and discussion

3.1. VIC model evaluation

Long-term averages of monthly streamflow are presented in Fig. 2 showing that seasonal peak streamflow generally occurs from early March to late May. Different watersheds, however, show different responses in winter and spring. For example, some watersheds in higher latitude areas including #1, 7, and 12 (hereafter number referring to a specific watershed ID number assigned in Table 1 and Fig. 1) show very rapid shifts from low streamflow in winter to extreme high flows in spring caused by cold winter temperatures, heavy snow accumulation, and large runoff volumes caused by rapid snowmelt in spring. These watersheds almost always flood in the spring. By contrast, more gradual increases in streamflow in spring can be found in lower latitude areas such as #4, 14 and 19. Peak flows in these watersheds are associated more with the general combination of elevated cool-season soil moisture and heavy precipitation events, and less with snowmelt, although snow accumulation and melt remain important contributing factors in some particular events. These warmer watersheds typically flood in the spring, but flooding is also common throughout the cold season from Nov–Mar (Fig. 3). It is important to note that the timing of peak monthly runoff averaged over a number of years (Fig. 2) and the timing of peak daily streamflow in any given year (Fig. 3) frequently coincide for colder snowmelt dominant watersheds, but often don't coincide for warmer watersheds in the southern parts of the domain. That is, the timing of flooding in snowmelt dominant watersheds is very consistent from year to year, whereas the timing of flooding in warmer watersheds is quite variable on an event basis.

Fig. 2 also compares composite means of monthly observed streamflow with simulations from the VIC HR. Although the model is not calibrated, the simulated magnitude and seasonal patterns of flow are quite similar with those observed in most watersheds. Validation statistics at monthly scale in Table 3 ($r > 0.85$ in most cases) further support these conclusions. However, it should be noted that the results in some watersheds show relatively poor agreement especially the timing of seasonal peak flow (e.g. #2 and 11). As noted earlier, these uncertainties in the simulations motivate us to focus on the ratio of future extreme streamflow relative to historically simulated streamflow, i.e. ratio of CCR to HR, rather than presenting absolute values of simulated extreme values.

For the evaluation of simulated extreme events, the seasonal timing and the magnitude of extreme events are both important physical and ecological drivers. Fig. 3 shows the timing and magnitude of daily peak streamflow values for observed and simulated data during each water year. For most watersheds, the VIC model does a good job of simulating the seasonal timing and approximate magnitude of flooding from first principles. This overall level of agreement is particularly remarkable given that the model has not been calibrated using the new V1 meteorological data set, and speaks to the model's ability to capture from first principles the diverse hydrologic mechanisms that cause flooding across the domain. This general agreement across different

watershed types with colder and warmer winters also speaks to the model's ability to capture changing conditions associated with regional warming and changes in precipitation. While doing a good job of simulating the overall response for many watersheds, streamflow in some watersheds are obviously overestimated (#8 and 13) or underestimated (#10 and 14). Validation statistics for peak flows (Table 3) shows more uncertainty introduced in peak daily streamflow compared to monthly values due to higher variability and finer temporal scale; however, simulated peak daily streamflow is well correlated with observed peak values, with r ranging from 0.6 to 0.87.

3.2. Projected changes in regional climate and hydrologic variables

Before investigating the impacts on hydrologic extremes, we first examine domain-averaged changes in key hydrologic variables that affect the seasonality and volume of streamflow. Fig. 4 shows projected changes of monthly hydrologic variables including precipitation (P), temperature (T), actual evapotranspiration (ET) and total column soil moisture (SM) for the 2020s, 2050s, 2080s relative to the averages for the historical baseline period ("No Change").

For P (Fig. 4a), substantial increases in winter and spring precipitation are projected, combined with a weak consensus from the GCMs regarding summer and fall precipitation. This basic pattern emerges by the 2020s, and steadily intensifies through time. Cold season (Dec–Apr) P is projected to increase significantly. For example, the ensemble mean of 6 GCMs for the 2080s RCP 8.5 scenario shows that P increases by about 30%. However, changes in warm season (Jun–Sep) P for the future periods do not appear to be statistically significant despite some stronger decreases at the end of century in August and September. Changes in P are not strongly different between the two GHG concentration scenarios.

For T changes (Fig. 4b), the GCMs project strong warming in all seasons, but especially in winter (Dec–Jan) and late summer (Aug–Sep). These basic patterns for T and P emerge in the 2020s and then strengthen through time. Changes in T by the 2080s are very intense, especially for the RCP8.5 scenario, which shows ensemble average T changes in excess of 6 °C, with the extreme high ranges in Dec and Aug approaching a change of 10 °C. These numbers are substantially higher than global mean values over land for the same time periods (Byun and Hamlet, 2018). For the 2020s there is no meaningful distinction between RCP4.5 and RCP8.5, but the difference in delta T between the two scenarios increases with time. There is a substantial difference of about 2 °C between the two concentration scenarios at the end of the century.

Actual ET (Fig. 4c) is likely to have distinctive seasonal changes which show increasing trends during spring (MAM) as well as late fall and early winter seasons (OND). By contrast, relatively minor changes during coldest (JF) and hottest periods (JJAS) are shown. Especially for this hottest period, water limitations due to decreased precipitation (Fig. 4a) may result in decreasing actual ET, despite strong increases temperature (Fig. 4b) and potential ET.

Changes in soil moisture (Fig. 4d) integrate changes in the other variables, and the results show decreasing patterns during summer and fall with small changes in the ensemble mean ($< -5\%$) for the 2080s. However, soil moisture is projected to systematically increase in winter, due to increasing precipitation (Fig. 4a) and more P falling as rain from Nov–Mar (Byun and Hamlet, 2018).

3.3. Future changes in seasonal streamflow

The patterns of regional climate change described above result in substantial changes in seasonal streamflow in many watersheds by the 2080s for the RCP8.5 scenario (Fig. 5). The results for RCP4.5 (Fig. S1) show consistent but smaller changes in comparison with RCP8.5. The following discussion relates to the RCP8.5 results in Fig. 5. Streamflow from Dec–Jan increases in all cases due to the combined

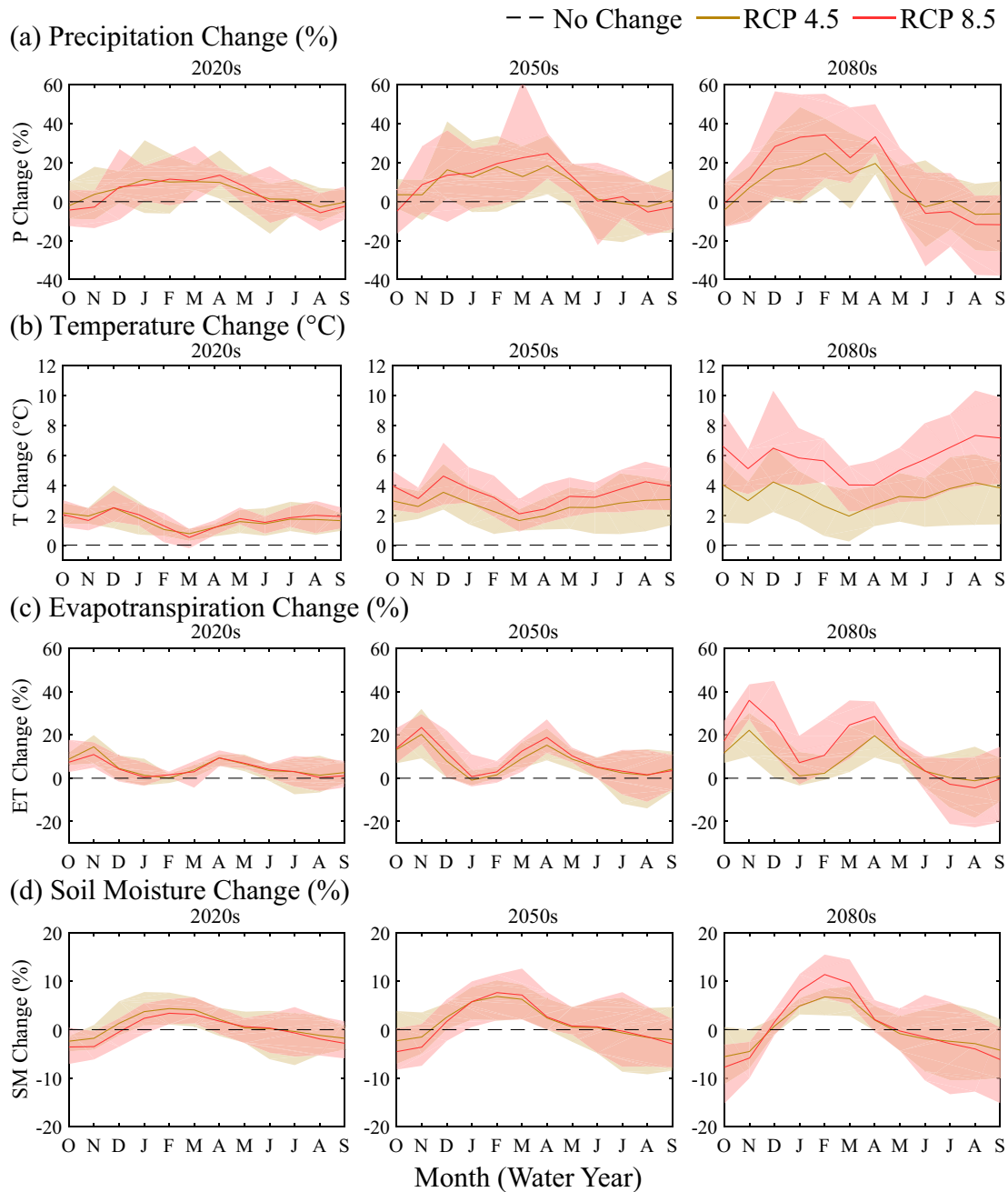


Fig. 4. Projected monthly changes in hydrometeorological variables over the whole region in Fig. 1: (a) Precipitation (P), (b) Temperature (T), (c) Evapotranspiration (ET) and (d) Soil Moisture (SM). P and T are derived from meteorological forcing data while ET and SM are simulated by VIC. Each shaded bound represents 95% confidence interval (2.5th to 97.5th percentile) and solid lines display the ensemble mean among 6 GCMs results.

effects of increasing P in winter and more P falling as rain. Twelve out of twenty watersheds examined (e.g. #8, 10, 14, 18) show increasing monthly peak flows and a characteristic shift towards peak flows occurring earlier in the year. In a smaller number of strongly snowmelt-dominant watersheds (e.g. #1, 17, 20), however, peak flows decline in response to the combined effects increasing T and P, because of reductions in SWE that are the main source of spring peak flows in these basins. Thus warmer watersheds that currently experience flood events throughout the winter and spring months are predominately projected to show increases in peak monthly run-off, whereas snowmelt-dominant watersheds that currently flood in spring, are projected to show reductions in monthly peak flows due to loss of spring snowpack.

These changes in seasonal streamflow timing suggest that there will likely be important changes in water resources impacts including water supply (municipal, industrial, and irrigation), hydropower production, and reservoir operating policies (Blöschl et al., 2017). Substantial increases in cool season streamflow shown in the results imply significant increases in hydropower production in run-of-river plants at this time of year, and suggest that increased generating capacity may be valuable in terms of maximizing energy production. Although we examined basins without major reservoirs, in other basins with dams and reservoirs, time sensitive reservoir operating policies (e.g. seasonal flood control operations) may need to be redesigned to account for the altered timing of refill and annual peak flows to ensure both reliable seasonal refill and effective flood control (see e.g. Lee et al., 2009).

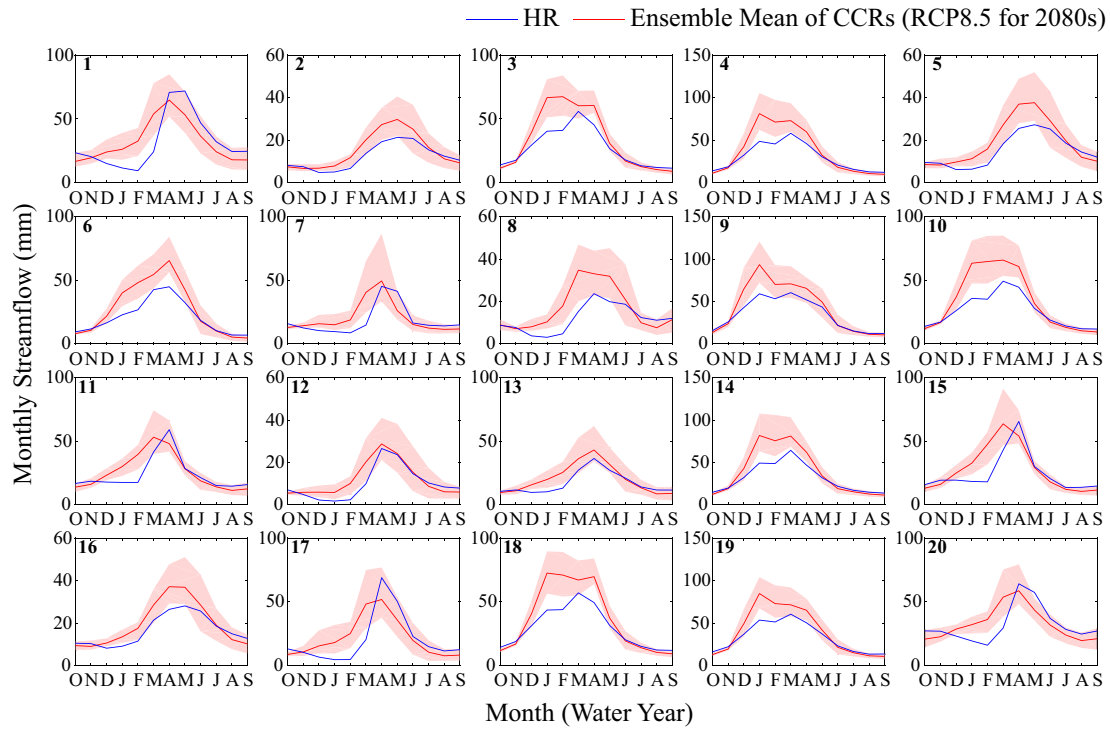


Fig. 5. Monthly streamflow at the outlets of each watershed by historical run (HR, blue solid line) and climate change runs (CCRs, ensemble mean with red solid line) of hydrologic simulation for RCP8.5 2080s. Each shaded range is bounded by minimum and maximum of 6 CCRs. Each panel represents the result for each watershed and the number in upper left corner matches to watershed ID number in Fig. 1 and Table 1.

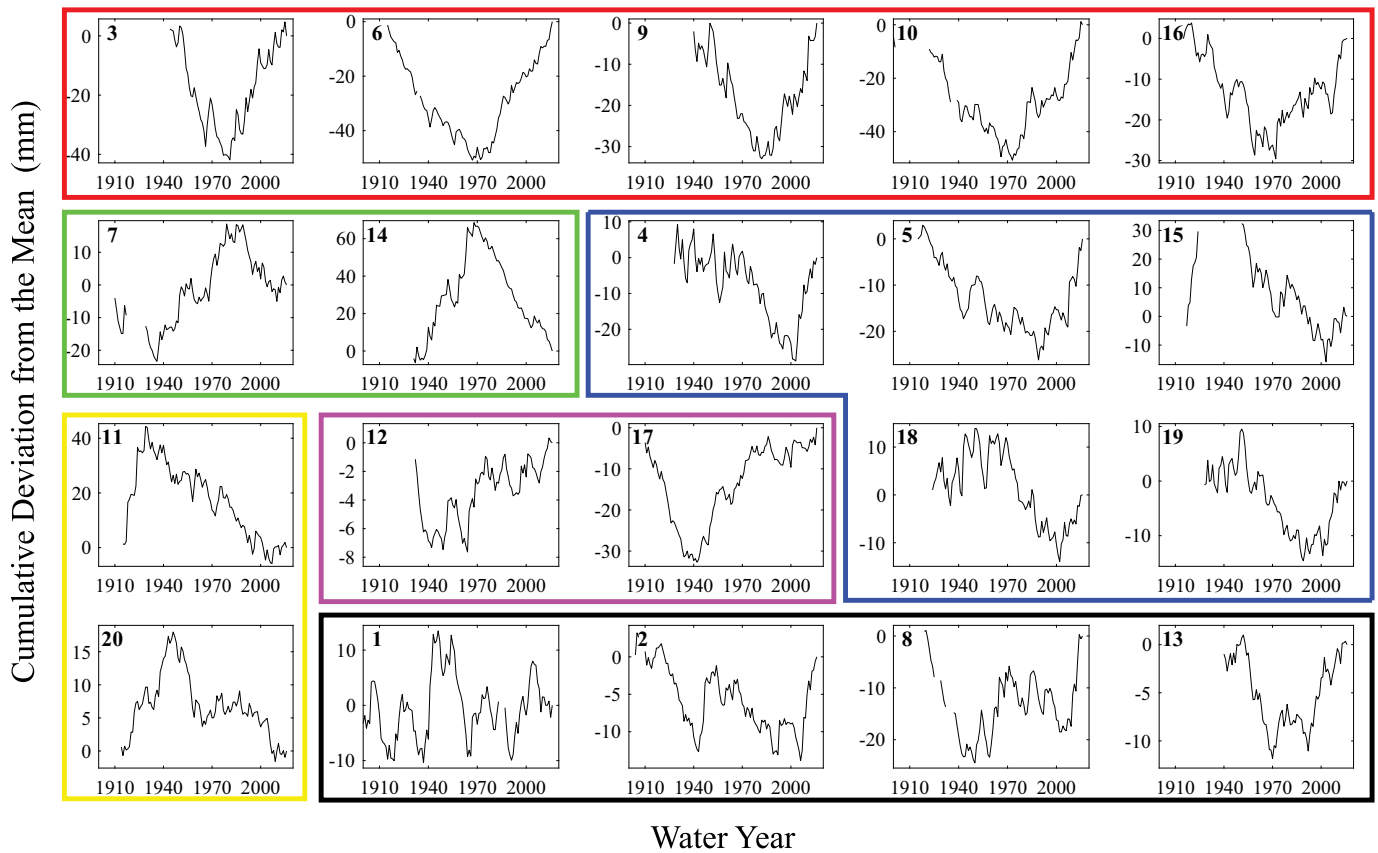


Fig. 6. Cumulative deviation from the mean of observed peak daily streamflow at the outlets (USGS gage station) of each watershed. Each panel represents the result for each watershed and the number in upper left corner matches to watershed ID number in Fig. 1 and Table 1. Also, results are grouped (colored bounds) based on their characteristics of regime shifts described in the text; Group 1 (red; 3, 6, 9, 10, and 16), Group 2 (green; 7 and 14), Group 3 (blue; 4, 5, 15, 18, and 19), Group 4 (purple; 12 and 17), Group 5 (yellow; 11 and 20) and Group 6 (black; 1, 2, 8, and 13).

3.4. Trends in observed peak daily streamflow

In order to investigate the long-term trends in peak daily streamflow from USGS observations, we calculate the CDM of peak daily streamflow for each water year from USGS observations using Eq. 5. As shown in Fig. 6, most watersheds show extended periods of peak streamflow above or below the long-term mean, in response to decadal-scale climate variability or other factors. Different watersheds show systematic changes in the mean during specific periods before and after some distinctive break points. For example, the results of CDM analysis for watersheds #3, 6, 9, 10, and 16 (Group 1) show a clear break point around 1975, with predominantly negative anomalies before about 1975 and predominantly positive anomalies after 1975. Watersheds #7 and 14 (Group 2) invert this breakpoint, with positive anomalies before 1975, and negative anomalies after 1975. Interestingly, this time period (roughly from 1975 forwards) is commonly considered as a critical transition point when warming due to radiative forcing associated with greenhouse gasses starts to emerge from the noise of natural variability (Hansen et al., 2010; IPCC, 2013). It is worth noting that this same breakpoint is present in other regions of the U.S. (e.g. the Pacific Northwest) as well.

Other watersheds (#4, 5, 15, 18, 19; Group 3), however, show a characteristic breakpoint around the year 2000, again with negative anomalies before 2000, and positive anomalies after 2000. Watersheds #12 and 17 (Group 4) show breakpoints around 1940 with negative anomalies before 1940 and positive anomalies after 1940. Watersheds #11 and 20 (Group 5) show breakpoints around 1940 with positive anomalies before 1940 and negative anomalies after 1940. Watersheds #1, 2, 8, and 13 (Group 6) are unusual in this group because they show no meaningful trends associated with decadal climate variability.

Interestingly, we found that geographic locations of watersheds with similar CDM patterns are not coherently distributed throughout the region. Thus, historical regime shifts in peak flows appear to be related to unique patterns of observed climate variability that affect

individual watersheds. This somewhat surprising result shows that hydrologic response to natural climate variability, combined with relatively small systematic climate changes in historical observations so far, retain strong local-scale components. In the future, however, as climate change impacts intensify, we hypothesize that impacts for individual watersheds may become more coherent.

3.5. Projected changes in peak daily streamflow

To analyze climate change impacts on extreme events, the values of peak daily streamflow for the HR and CCR were used to estimate the parameters of the GEV distribution, and changes in the estimated 100-yr events in the future were evaluated relative to the historical baseline (Fig. 7). Floods risk in most watersheds is projected to increase, and the changes in projected flood risk are greater for RCP 8.5 than for RCP 4.5. For watersheds with increasing flood risks, these risks often intensify through time in the projections. This may result from steadily increasing precipitation during winter and spring seasons in the future which will likely affect peak streamflow in those seasons.

However, when we focus on 2080s some watersheds (e.g. #7, 11, 13, 15, 17 and 20) show decreasing intensity of extreme events for the majority of CCRs. These watersheds are all strongly snowmelt dominant watersheds in the northern part of the domain that flood in spring due to heavy snowmelt (see Fig. 5). With winter warming, spring snow-pack decreases, and so do the spring peak flows, thus reducing flood risk.

Despite some differences among watersheds, the peak timing for the ensemble mean of CCRs is shifted earlier than that of HR in all 20 watersheds without exception (Fig. 8), and these earlier shifts generally intensifying with time are statistically significant in most cases by the 2080s. It is also worth noting that the watersheds that show decreases in peak daily streamflow (e.g. #7, 17 and 20) show more significant timing shifts (< -30 days) compared to the majority of watersheds that show increasing flood risks. This is presumably because the

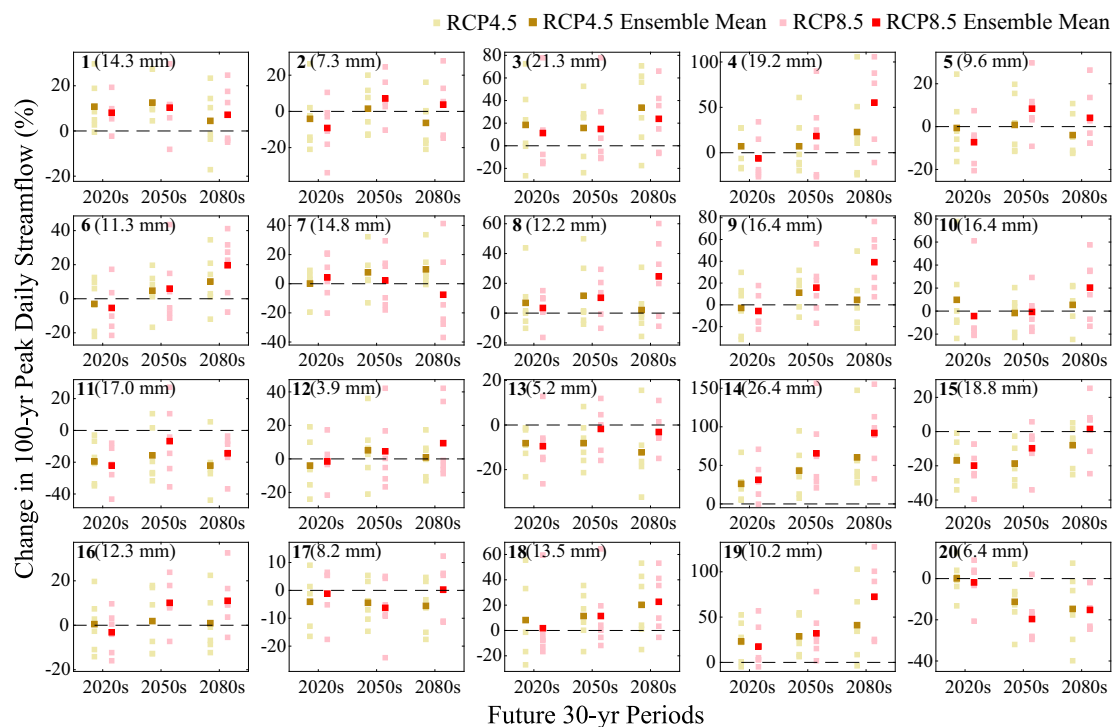


Fig. 7. Changes (%) in peak daily streamflow with 100-yr return interval at the outlets of each watershed for 3 future 30-yr periods (x-axis). Each individual CCR is represented as light colored markers (olive and pink for RCP4.5 and RCP8.5, respectively) and ensemble mean of CCRs are shown as darker markers. Each panel represents the result for each watershed and the number in upper left corner matches to watershed ID number in Fig. 1 and Table 1. Also, numbers in the parenthesis represent observed peak daily streamflow with 100-yr return interval at the USGS stations.

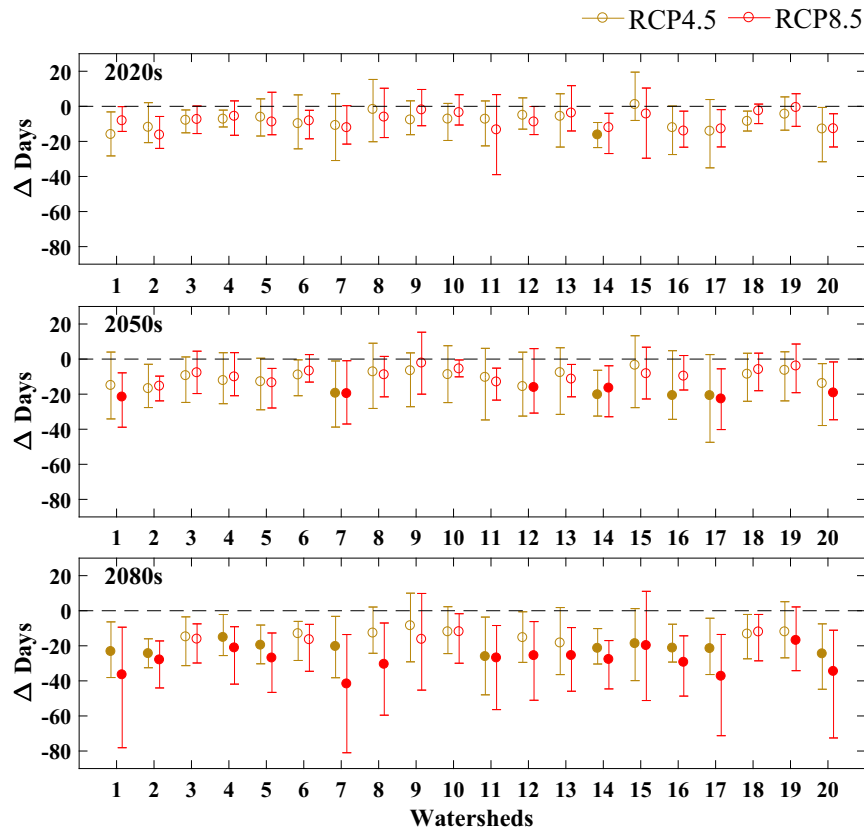


Fig. 8. Changes in timing of peak daily streamflow (days, y-axis) at the outlets of each watershed (x-axis) for 3 future periods (upper-2020s, middle-2050s and lower-2080s). Each bar is bounded by minimum and maximum of 6 CCRs and circle represents ensemble mean of CCRs. Two samples *t*-test is conducted for comparing between HR and ensemble mean of CCRs, and marker filled with color represents statistical significance ($\sigma = 0.05$).

watersheds with the greatest timing shifts are most dependent on the seasonal timing of peak snowmelt, which we show in the subsequent section moves substantially earlier in the year in these watersheds, whereas the watersheds with increasing flood risks are responding both to shifts from snow to rain (T) and increasing winter and spring P impacts which have a less clear cut temporal signature in the results.

These changes have important implications in many different sectors. Increasing flood risk over time threatens existing homes and businesses, determines where new structures may be built, and increases risks to public safety due to flood inundation, transportation impacts, and effects to public services such as fire response and hospitals. Infrastructure such as bridges, levees, and dams may need to be strengthened or redesigned to cope with changing flood risks, and new design standards that incorporate non stationary statistics will need to be developed to account for changing probability distributions over time. Long-lived infrastructure (such as bridges and levees) may be particularly vulnerable to these kinds of changes.

Increasing flood risk can also result in harmful effects in urban environment due to flash flooding and overflow of combined sewer systems into rivers and lakes (Jagai et al., 2015), and increased transports of nutrients from agricultural fields during extreme events in winter will likely impact downstream water bodies such as the Great Lakes and Gulf of Mexico (Ockenden et al., 2016). Thus, adaptive environmental strategies for coping with changing risks of extremes are needed to effectively regulate and control contaminant sources in both urban and agricultural areas.

3.6. Projected changes in annual maximum SWE and its impacts on peak streamflow

To diagnose the cause of projected changes in peak daily streamflow in different watersheds, we analyze annual maximum SWE, which plays

a crucial role in peak streamflow during spring, especially in snowmelt-dominated watersheds. As shown in Fig. 9a and c, by the 2080s annual maximum SWE is projected to decrease by about 50% over the whole domain. This is consistent with reductions in the fraction of precipitation falling as snow during cold season shown by Byun and Hamlet (2018). These reductions in peak SWE point to a declining contribution of snowmelt to flooding, but as described previously, total precipitation during winter and spring season is projected to increase substantially ($<+40\%$ at the end of century), which can readily cancel out the decreasing contribution of snowmelt to peak streamflow. Furthermore, due to projected warming, many watersheds may not hold snow on the ground until spring season, which means that characteristics of storm events (e.g. rain vs. snow, intensity, and inter-arrival time) during winter and spring will likely have a more important influence on the behavior of peak streamflow, especially in the southern parts of the domain.

Fig. 9 confirms this, and shows that the timing of peak SWE occurs substantially earlier in the higher latitude areas but changes very little in the low latitude areas. It is also clear that the watersheds in the higher latitudes usually hold snow a longer time and peak streamflows are caused by snowmelt rather than extreme P. Thus, earlier snowmelt in this type of watersheds will essentially result in earlier timing shift in peak streamflow. Aforementioned results showing the changes in seasonal peak streamflow (Fig. 5) and peak daily streamflow (Fig. 7) support this conclusion. For example, most watersheds that have decreasing trends in peak streamflow with critical earlier timing shift (#7, 11, 13, 15, 17 and 20) are located in the higher latitudinal areas where annual maximum SWE is projected to change substantially in both magnitude and timing. In contrast, watersheds showing higher flood risks have relatively minor changes in timing of annual maximum SWE. Thus the majority of watersheds in this study are less affected by

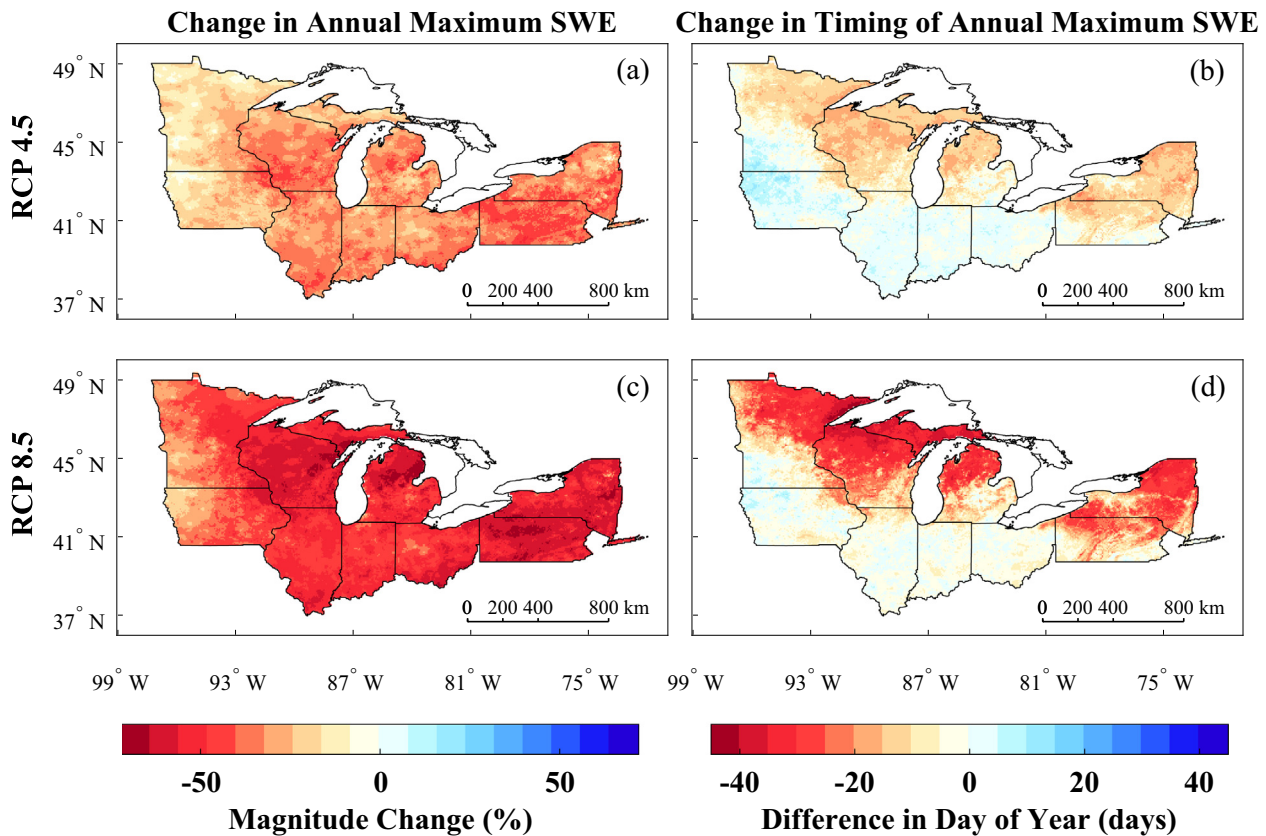


Fig. 9. Changes in magnitude (%; left column) and timing (days; right column) of annual maximum SWE by ensemble mean of CCRs based on RCP4.5 (upper row) and RCP8.5 (lower row) for 2080s.

peak snow accumulation in spring, and instead are most substantially affected by projected increases in precipitation as rainfall during cold season.

3.7. Effects of changing initial SM on flooding

Changing flood risks are a complex interaction between changing P and snowmelt dynamics, and initial SM conditions. In basins that typically flood in response to intense rainfall in spring, the effects of changing P type, earlier snowmelt, and increasing P on flood risk (discussed above) are generally exacerbated by systematic increases in antecedent SM conditions in the simulations (Fig. 4d and Fig. S2), because elevated SM increases baseflows, reduces infiltration capacity, and therefore increases surface runoff in the simulations. This also partly explains why snowmelt dominant basins tend to show relatively little change in flood risk overall. Loss of snowcover reduces surface water availability in spring when flooding occurs, but SM is also higher, which opposes these changes.

Fig. S2 shows the general increasing trends in soil moisture in most watersheds, especially in late winter and early spring. In the VIC simulations, increasing SM is attributable to increasing trends of P as rainfall, and early melting of snowpack, but in the real system less frequent occurrence of frozen soils may also contribute to increased infiltration and elevated soil moisture in winter. Thus reductions in frozen soil may reduce flooding in mid-winter by increasing infiltration capacity, but may subsequently increase flood risk in late winter and early spring due to elevated SM. Changes in the timing of peak SM also affects the timing of flooding shown in the simulations by changing the coincident timing between heavy spring P as rain (or snowmelt) and elevated SM. For example, timing of peak SM in several snowmelt-dominated watersheds (#1, 7, 17 and 20 in Fig. S2) shows significant shifts, and results for this watershed type also showed substantial shifts in timing of peak

flows as discussed earlier (Fig. 8). By contrast, most watersheds that show increasing flood risks with relatively small timing shifts also do not show significant timing shifts in SM. Thus, changes in flood risk in these basins likely depend primarily on the changing seasonality of P (Fig. S3), and systematic changes from snow to rain. In particular, a number of the warmer southern watersheds (e.g. #4, 9, 14, 19 in Fig. S3) show pronounced increases in P in winter and spring, whereas most snowmelt dominant basins show modest (and approximately equal) percent changes throughout the cool season (e.g. #1, 2, 7, 17, 20). These same effects on the seasonal timing and amount of infiltration and resulting baseflows can also affect the seasonal timing of low flows in some basins, as discussed in more detail below.

Although the effects vary considerably in different basins, in general there are systematic increases in winter and spring SM that suggest increased difficulty in draining agricultural areas in spring, and also increased soil erosion and transport of nutrients from agricultural areas throughout the cool season. Adaptive strategies such as the planting of cover crops may help to avoid some of these impacts (Hanrahan et al., 2018), but further study is needed to quantify these impacts at the watershed scale.

3.8. Projected changes in 7-day low streamflow

For the extreme low-flow analysis, we extracted the values of the lowest 7-day averaged streamflow for each water year from the simulations and fitted parameters for the GEV distribution to these data. Fig. 10 shows the changes in extreme 7-day low streamflow events with 10-yr return interval (7Q10) for each watershed. Although there is considerable variability from site to site, for different RCPs and future periods, in most watersheds there are increasing trends in extreme low streamflow in the future. For example, many watersheds show moderate increasing trends (<+10%) in the ensemble mean of 7-day extreme

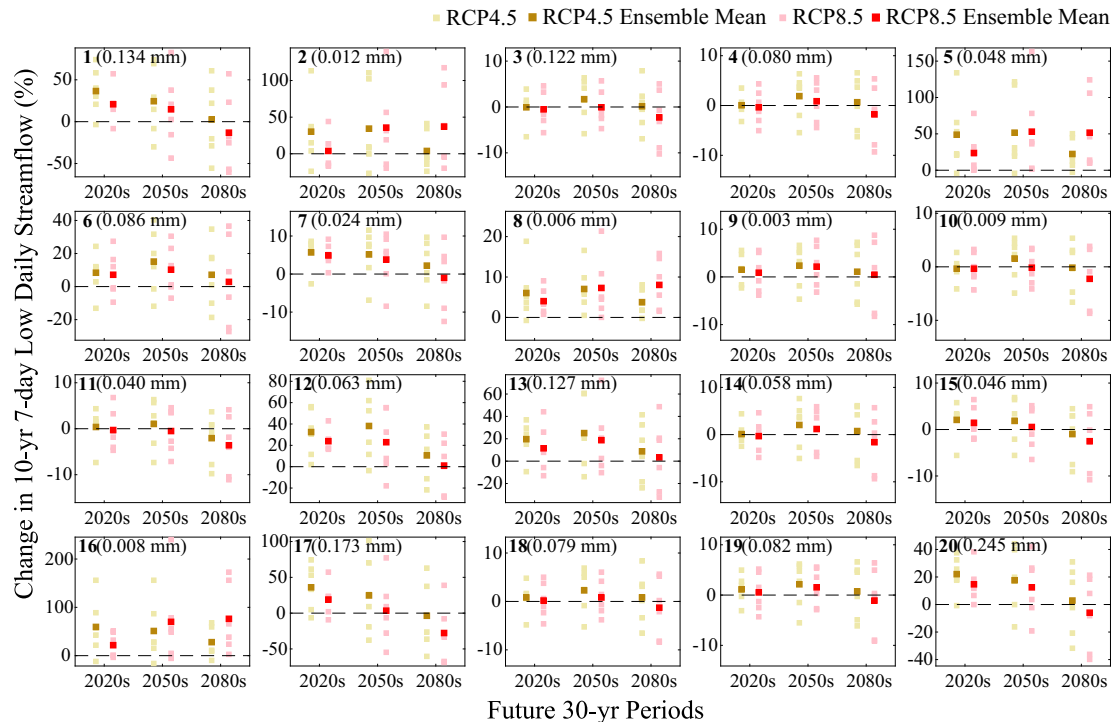


Fig. 10. Changes (%) in extreme 7-day low streamflow with 10-yr return interval (7Q10) at the outlets of each watershed for 3 future 30-yr periods (x-axis). Each individual CCR is represented as light colored markers (olive and pink for RCP4.5 and RCP8.5, respectively) and ensemble mean of CCRs are shown as darker markers. Each panel represents the result for each watershed and the number in upper left corner matches to watershed ID number in Fig. 1 and Table 1. Also, numbers in the parenthesis represent observed 7Q10 at the USGS stations.

low flows, while some watersheds (e.g. #2, 5 and 16) show more significant increasing patterns (<+50%), especially for the 2020s and 2050s. However, this increase in extreme low flow events is substantially reduced, or even reversed to show reductions in extreme low flows, by the 2080s. This decreasing pattern for the 2080s is related to P changes during late summer and early fall season (Fig. 4), which shows modest reductions at the end of century in the ensemble mean. Because there is not a strong consensus between models regarding summer and fall P changes (Byun and Hamlet, 2018), the same basic uncertainties apply to low flows as well. That is, some GCMs project conditions that result in higher low flows in the hydrologic simulations, some lower.

Although the magnitude and timing of extreme low flows does not change markedly in many watersheds, the timing of low flow events changes substantially in relatively cold, snowmelt dominant watersheds. To show these changes, we focus on the probability density of the timing of each year's low extreme represented as day of year in water year sequence. For example, Fig. 11 shows the timing of 7-day extreme low streamflow in the Wisconsin River watershed (#20 in Fig. 1). Historically extreme low flow occurs in three distinctive time frames: mid-summer to early fall (280–365 day of water year), mid fall (0–50 day of water year) and late winter to early spring (120–180 day of water year). In a warmer and wetter climate, winter/spring low flows become increasingly rare and the number of late summer and fall events increases. Similar patterns of change were found in other snowmelt dominant basins (e.g. #1 and 7). Winter/spring extreme low flows are historically expected in very cold basins, due to deep snowpack, frozen soils, an extended period of drainage without recharge, and resulting low soil moisture. However, these conditions become less frequent in cold basins under changing climate in the simulations, and the timing of extreme low flows shifts to late summer and early fall, effectively mirroring the behavior of warmer watersheds at lower latitudes.

Decreasing extreme low flows projected for the end of the century are probably most important in the context of aquatic ecosystem

impacts, recreational impacts, and hydropower production. More intense low flows, for example, can reduce habitat for fish and wildlife, increase water temperature, or increase contaminant or nutrient concentrations, leading to impacts such as harmful algal blooms,

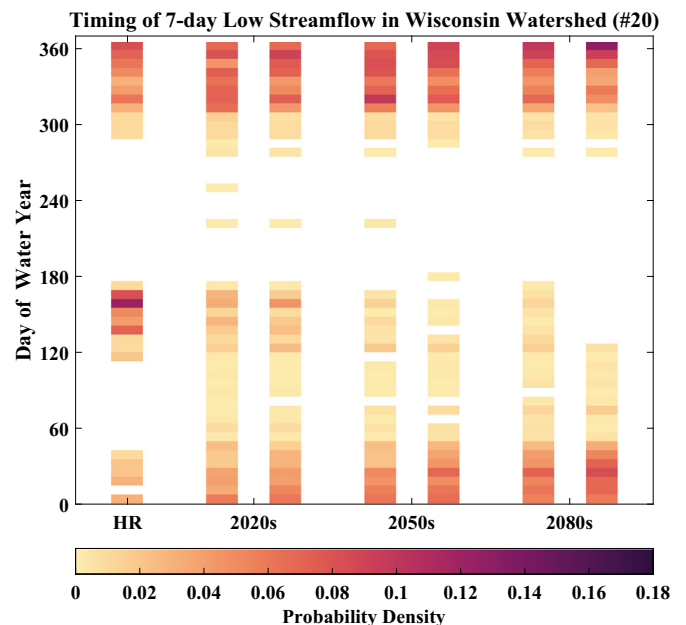


Fig. 11. Timing (Day of Water Year, y-axis) of 7-day low streamflow at the outlets of the Wisconsin River watershed (#20 in Fig. 1) for historical and three future 30-yr periods (x-axis). Probability density was calculated by counting number of extreme low flow events in each 7-day bin and normalizing it by the total number of events. The results of HR are represented in the first column while those of CCRs based on RCP4.5 and RCP8.5 are shown in left and right column in each future period, respectively.

beach closures (e.g. in response to e-coli concentrations in downstream water bodies), or other water quality violations. More intense low flows may have substantial impacts on recreational activities such as fishing, swimming and boating in rivers, and may impact the capacity of hydro-power production in late summer, particularly for run-of-river hydro-power plants, and power plants that use river water for cooling.

3.9. Projected change in 7-day low soil moisture (SM)

Fig. 12 shows the projected % changes in the magnitude of the ensemble mean of 7-day extreme low SM by CCRs over the Midwest and Great Lakes region. The change in 7-day low SM is consistent with the 7-day low streamflow analysis. For example, up to 2050s most areas show moderate increasing trends in extreme low SM ($<+10\%$) regardless of RCPs; however, modest negative changes are projected for the 2080s in most areas except Illinois and southern parts of Pennsylvania. The largest decrease in simulated extreme low SMs are in the northern most parts of the domain (e.g. northern MI, WI and NY). These impacts are probably related to loss of heavy snow cover in the future simulations in these areas, resulting in reduced soil moisture in spring and an effectively longer summer drying period with increased ET (as discussed in Section 3.7). Winter SM, however, tends to systematically increase in the same basins.

We also found that spatially averaged extreme low SM was reasonably well correlated with extreme low flow at the watershed scale and shows similar projected changes, which suggests a possible approach for estimating ungauged streamflow at the outlet point of basin where soil moisture measurements are available (e.g. in agricultural settings) or for estimating relative soil moisture impacts from observed low flows.

Decreased SM extremes, especially when coupled with elevated heat stress, can cause irreparable crop damage. One adaptive response to cope with this impact is increased use of irrigation. However, widespread use of irrigation will have substantial economic costs to the region, and increased irrigation may also result in lowered groundwater levels, indirectly impacting baseflows in streams (Wang and Cai, 2010). Thus, increased irrigation in response to SM impacts, may ultimately impact low flows and ecosystem health in streams.

3.10. Sources of uncertainty

Although the fundamental uncertainty in climate projections from two emissions scenarios and multiple GCMs (each with its unique sensitivity to global greenhouse forcing) is explicitly explored by Byun and Hamlet (2018), it is worth noting that there are many other potential sources of uncertainty in our hydrologic modeling framework. These include choice of statistical downscaling approach, hydrologic model and routing model structure and parameter uncertainty, and unexplored changes in land cover, changes in human water use over time, and the Great Lakes themselves.

3.10.1. Hydrologic model uncertainty

In most studies that have explicitly explored the effects of climate and hydrologic model structure and parameter uncertainty on hydrologic extremes, the magnitude of hydrologic modeling uncertainties are typically smaller than those related to climate (see e.g. Wilby et al., 2009; Mendoza et al., 2015), especially when model bias is taken into account in interpreting the results (i.e. when results are expressed as percent changes instead of absolute values). For example, Tohver et al. (2014) showed that the sensitivity of simulated hydrologic extremes to projected changes in T and P (e.g. percent changes in the 100-year flood) were relatively insensitive to calibration of the VIC routing model, even though the absolute value of the model results changed markedly after calibration. Thus, any future calibration of the VIC model or routing model is not expected to substantially change the results presented here. Also, our validation results (Figs. 2 and 3 and Table 3) show reasonable performance of the VIC model in reproducing observed seasonal and extreme streamflow, which again supports the argument that uncertainties associated with climate projections are likely to be more significant factors than calibration of the hydrologic model. Use of other hydrologic models, however, might introduce different sensitivity to changes in T and P, which could expand the range of uncertainty shown in our results.

3.10.2. Changes in summer precipitation

Projected changes in summer precipitation are especially uncertain in this study both because of a lack of GCM consensus on systematic change (Byun and Hamlet, 2018), and also because of the inability of

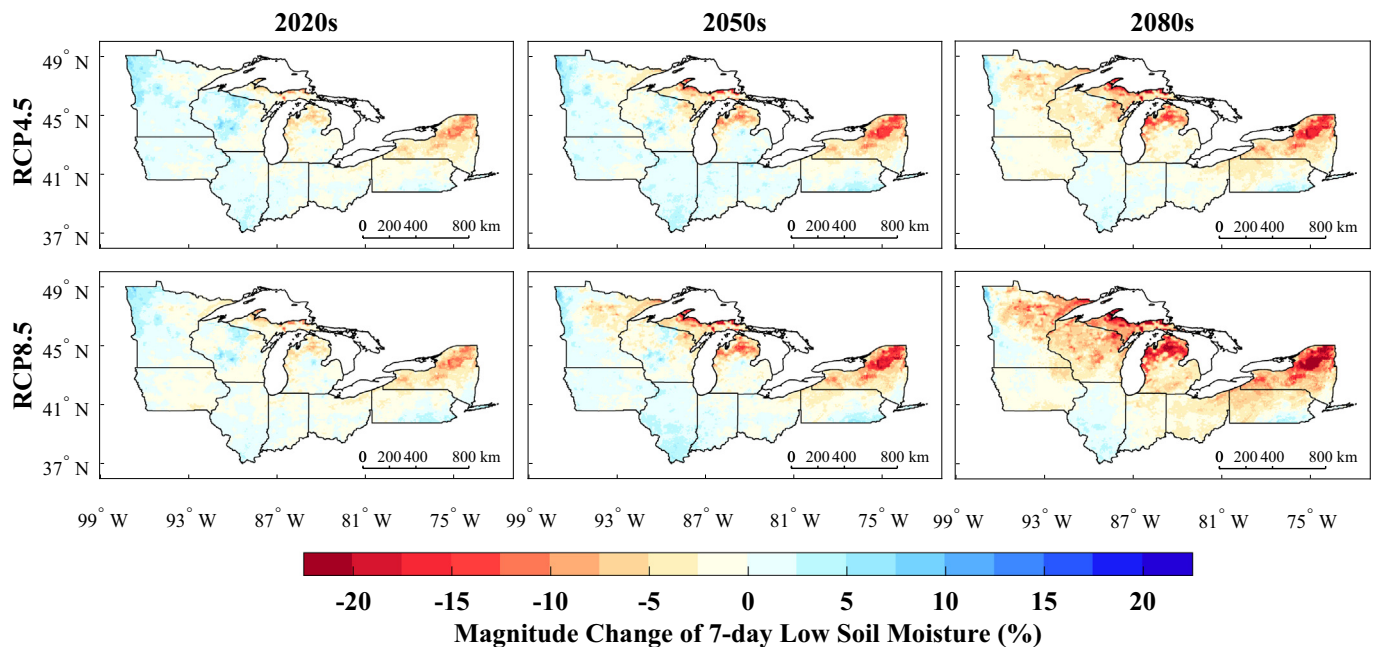


Fig. 12. Simulated changes in the magnitude (%) of ensemble-mean of 7-day low SM based on RCP4.5 (upper row) and RCP8.5 (lower row) for 3 future periods (left-2020s, middle-2050s and right-2080s).

GCM's to capture small-scale convective storms (Ahn and Kang, 2018) that are the main source of precipitation in warm season. Uncertainties in the Great Lakes themselves are also not well captured by the GCMs, which has important implications for many kinds of impacts studies, including assessment of changing extremes (Byun and Hamlet, 2018; Sharma et al., 2018). Thus, high-resolution regional climate models dynamically incorporating the Great Lakes are needed to explore these effects in more detail. Such tools could give substantially different results than those shown here (Sharma et al., 2018), especially in summer.

3.10.3. Changes in natural vegetation, crop type, and human water use

Dynamic changes in vegetation and human water use are not included in either the GCMs or the hydrologic models used in this study. The regional-scale results compiled by Byun and Hamlet (2018) suggest that annual average T changes on the order of 10 °C are possible by 2100. The sheer magnitude of these temperature impacts suggests that important (and so far largely unexplored) changes in forests, rangeland, and agriculture in the Midwest region will accompany regional warming. For example, increased disturbance to forests due to fire or disease could increase savannah or prairie land cover type, or could systematically increase deciduous forest cover. Reductions in tree cover could reduce canopy interception and ET, resulting in increased soil moisture and high-flow extremes. Hotter (and perhaps drier) summers could result in changes in agricultural production (crop type) or irrigation practices (Bowling et al., 2018), affecting hydrologic extremes. For example, increased use of irrigation in summer could systematically reduce groundwater levels resulting in reduced baseflow to streams and so more significant extreme low flows in late summer.

The issues discussed above and some other discussions on the uncertainty of hydrologic projections by Melsen et al. (2018) highlight the fact that despite our attempt to characterize some of the most important climate uncertainties, the range of uncertainty shown in our results probably understates the full range of uncertainty associated with our integrated modeling framework, and this should be taken into account in interpreting the results.

4. Summary and conclusions

Modeling hydrologic extremes is a challenging task because of their complex and non-linear response to climate, and the seasonal characteristics of regional climate change adds even more complexity to the modeling of future hydrologic extremes. This study projects future hydrologic extremes using a macro-scale hydrologic model forced by downscaled GCM datasets in 20 watersheds over the Midwest and Great Lakes region.

Cumulative deviation from the mean plots of observed extreme streamflow show some common break points around 1970 to 2000 in many watersheds, which suggest that the flow regime has experienced a relatively abrupt and persistent shift towards higher peak flows in this period. Decadal climate variability and systematic changes related to climate change are likely causes of this behavior, and are broadly consistent with what we expect in the future from regional climate change. Other watersheds, however, show different patterns that are not consistent with expected climate change responses.

We summarize several key elements of the study results, but it should be noted that projected changes in hydrologic extremes are site-specific, and vary with different hydrologic characteristics.

1. Annual maximum SWE is projected to decrease significantly due to regional warming. Precipitation falling as rain increases. There will be significant timing shifts of melting snow towards earlier spring, especially in snowmelt-dominant watersheds.
2. Peak daily streamflow generally increases (RCP8.5 at 2080s, +10–30%) due to significant increasing precipitation during winter and spring seasons, however some snowmelt-dominated

watersheds show decreasing trends or little change. Snowmelt-dominant basins also tend to show a pronounced shift in seasonal peak flow timing towards earlier dates in the water year in response to warming. Other basins show relatively modest changes in peak flow timing.

3. 7-day extreme low streamflow is projected to increase moderately at the beginning of the 21st century (<+10%), and decrease more substantially at the end of 21st century (<−20%) in many watersheds. The timing of extreme low flows changes substantially in snowmelt watersheds, with extremes occurring less frequently in winter and spring, and more often in late summer and early fall.
4. Projected changes in 7-day low SM are largest in the northernmost parts of the domain, and are strongly correlated with changes in 7-day low streamflow in the simulations.

Results of this study suggest that future hydrologic extremes will likely bring detrimental effects on natural ecosystems as well as human society. For example, increasing peak streamflow will likely create higher risks to dwellings, businesses, water infrastructure, and human safety, due to increased river flooding events during cold season. Also, in the absence of adaptive actions, increased surface runoff in winter season may result in increased nutrient loading from agricultural areas (due to loss of snowpack and increased precipitation intensity as rain), which can ultimately lead to severe ecosystem disturbances, such as harmful algal blooms in downstream receiving water bodies. Strongly snowmelt-dominant watersheds in the northern parts of the domain (e.g. # 1, 7, and 20) showed substantial changes in the timing of seasonal floods (Fig. 8), and also the timing of extreme low flows (Fig. 11). By the 2080s, the lack of a strong spring freshet in these basins, combined with decreasing extreme low flows in late summer, is likely to have profound ecological consequences.

In the context of analyzing hydrologic extremes, future analysis should focus on the non-stationarity of extremes through time in order to derive more statistically robust and realistic values needed to inform long-range planning and the design of infrastructure. Furthermore, despite a few exploratory studies to date (Naz et al., 2016; Schwartz et al., 2017; Wang et al., 2014), additional hydrologic modeling and analysis using dynamically-downscaled forcing datasets are needed to better capture the changing nature of small-scale convective storms, which will likely impact both high- and low-flow extremes, especially in summer.

Acknowledgements

Thanks to Gonzalo Huidobro Marin, guest undergraduate researcher at the University of Notre Dame, for his work in developing and validating the 1/16th degree routing network and direction file used in this study. The research in this paper was supported by The Department of Civil and Environmental Engineering and Earth Sciences and the Environmental Change Initiative at the University of Notre Dame.

Appendix A. Supplementary data

Supplementary data (Table S1 and Figure S1–S3) to this article can be found online at <https://doi.org/10.1016/j.scitotenv.2018.09.063>.

References

- Ahn, M., Kang, I., 2018. A practical approach to scale-adaptive deep convection in a GCM by controlling the cumulus base mass flux. *Clim. Atmos. Sci.* 1 (13). <https://doi.org/10.1038/s41612-018-0021-0>.
- Barnett, T.P., Pierce, D.W., Hidalgo, H.G., Bonfils, C., Santer, B.D., Das, T., Bala, G., Wood, A.W., Nozawa, T., Mirin, A.A., 2008. Human induced changes in the hydrology of the western United States. *Science* 319, 1080. <https://doi.org/10.1126/science.1152538>.
- Bennett, K.E., Cannon, A.J., Hinzman, L., 2015. Historical trends and extremes in boreal Alaska river basins. *J. Hydrol.* 527, 590–607. <https://doi.org/10.1016/j.jhydrol.2015.04.065>.

- Blöschl, G., Hall, J., Parajka, J., Perdigão, R.A.P., Merz, B., Arheimer, B., Aronica, G.T., Bilibashi, A., Bonacci, O., Borga, M., Ivan, Č., Castellarin, A., Chirico, G.B., 2017. European floods. *Science* 357, 588–590. <https://doi.org/10.1126/science.aan2506>.
- Bowling, L.C., Widhalm, M., Cherkauer, K.A., Beckerman, J., Brouder, S., Buzan, J., Doering, O., Dukes, J., Ebner, P., Frankenburger, J., Gramig, B., Klavivko, E.J., Lee, C., Volenc, J., Weil, C., 2018. Indiana's Agriculture in a Changing Climate: A Report from the Indiana Climate Change Assessment. Agriculture Reports. Paper 1. <https://doi.org/10.5703/1288284316778>.
- Byun, K., Hamlet, A.F., 2018. Projected changes in future climate over the Midwest and Great Lakes region using downscaled CMIP5 ensembles. *Int. J. Climatol.* 38 (Suppl.1), e531–e553. <https://doi.org/10.1002/joc.5388>.
- Cayan, D.R., Das, T., Pierce, D.W., Barnett, T.P., Tyree, M., Gershunov, A., 2010. Future dryness in the southwest US and the hydrology of the early 21st century drought. *Proc. Natl. Acad. Sci. U. S. A.* 107, 21271–21276. <https://doi.org/10.1073/pnas.0912391107>.
- Chen, J., Brissette, F.P., Poulin, A., Leconte, R., 2011. Overall uncertainty study of the hydrological impacts of climate change for a Canadian watershed. *Water Resour. Res.* 47, 1–16. <https://doi.org/10.1029/2011WR010602>.
- Cherkauer, K.A., Sinha, T., 2010. Hydrologic impacts of projected future climate change in the Lake Michigan region. *J. Great Lakes Res.* 36, 33–50. <https://doi.org/10.1016/j.jglr.2009.11.012>.
- Chien, H., Yeh, P.J.F., Knout, J.H., 2013. Modeling the potential impacts of climate change on streamflow in agricultural watersheds of the Midwestern United States. *J. Hydrol.* 491, 73–88. <https://doi.org/10.1016/j.jhydrol.2013.03.026>.
- Chiu, C.-M., Hamlet, A.F., Byun, K., Macro-scale precipitation gauge undercatch corrections for the Midwest and Great Lakes region.
- Demaria, E.M.C., Palmer, R.N., Roundy, J.K., 2016. Regional climate change projections of streamflow characteristics in the Northeast and Midwest U.S. *J. Hydrol. Reg. Stud.* 5, 309–323. <https://doi.org/10.1016/j.ejrh.2015.11.007>.
- Doney, S.C., Ruckelshaus, M., Emmett Duffy, J., Barry, J.P., Chan, F., English, C.A., Galindo, H.M., Grebmeier, J.M., Hollowed, A.B., Knowlton, N., Polovina, J., Rabalais, N.N., Sydeman, W.J., Talley, L.D., 2012. Climate change impacts on marine ecosystems. *Annu. Rev. Mar. Sci.* 4, 11–37. <https://doi.org/10.1146/annurev-marine-041911-111611>.
- Fischer, G., Tubiello, F.N., van Velthuisen, H., Wiberg, D.A., 2007. Climate change impacts on irrigation water requirements: effects of mitigation, 1990–2080. *Technol. Forecast. Soc. Chang.* 74, 1083–1107. <https://doi.org/10.1016/j.techfore.2006.05.021>.
- Haddeland, I., Heinke, J., Biemans, H., Eisner, S., Flörke, M., Hanasaki, N., Konzmann, M., Ludwig, F., Masaki, Y., Schewe, J., Stacke, T., Tessler, Z.D., Wada, Y., Wisser, D., 2014. Global water resources affected by human interventions and climate change. *Proc. Natl. Acad. Sci. U. S. A.* 111, 3251–3256. <https://doi.org/10.1073/pnas.1222475110>.
- Hamlet, A.F., Elsner, M.M., Mauger, G., Lee, S.-Y., Tohver, I., 2013. An overview of the Columbia Basin climate change scenarios project: approach, methods, and summary of key results. *Atmosphere-Ocean* 51, 392–415. <https://doi.org/10.1080/07055900.2013.819555>.
- Hanrahan, B.R., Tank, J.L., Christopher, S.F., Mahl, U.H., Trentman, M.T., Royer, T.V., 2018. Winter cover crops reduce nitrate loss in an agricultural watershed in the central U. S. *Agric. Ecosyst. Environ.* 265, 513–523. <https://doi.org/10.1016/j.agee.2018.07.004>.
- Hansen, J., Ruedy, R., Sato, M., Lo, K., 2010. Global surface temperature change. *Rev. Geophys.* 48 (RG4004). <https://doi.org/10.1029/2010RG000345>.
- Hattermann, F.F., Krysanova, V., Gosling, S.N., Dankers, R., Dagguapati, P., Donnelly, C., Flörke, M., Huang, S., Motovilov, Y., Buda, S., Yang, T., Müller, C., Leng, G., Tang, Q., Portmann, F.T., Hagemann, S., Gerten, D., Wada, Y., Masaki, Y., Alemayehu, T., Satoh, Y., Samaniego, L., 2017. Cross-scale intercomparison of climate change impacts simulated by regional and global hydrological models in eleven large river basins. *Clim. Chang.* 141, 561–576. <https://doi.org/10.1007/s10584-016-1829-4>.
- Hay, L.E., Markstrom, S.L., Ward-Garrison, C., 2011. Watershed-scale response to climate change through the twenty-first century for selected basins across the United States. *Earth Interact.* 15, 1–37. <https://doi.org/10.1175/2010EI370.1>.
- Hayhoe, K., Vandorn, J., Croley, T., Schlegel, N., Wuebbles, D., 2010. Regional climate change projections for Chicago and the US Great Lakes. *J. Great Lakes Res.* 36, 7–21. <https://doi.org/10.1016/j.jglr.2010.03.012>.
- Hirsch, R.M., Ryberg, K.R., 2012. Has the magnitude of floods across the USA changed with global CO₂ levels. *Hydrol. Sci. J.* 57, 37–41. <https://doi.org/10.1080/02626667.2011.621895>.
- Hosking, J.R.M., Wallis, J.R., 2005. *Regional Frequency Analysis: An Approach Based on L-Moments*. Cambridge University Press.
- Hosking, J.R., Wallis, J.R., Wood, E.F., 1985. Estimation of the generalized extreme-value distribution by the method of probability-weighted moments. *Technometrics* 27, 251–261. <https://doi.org/10.1080/00401706.1985.10488049>.
- Howden, S.M., Soussana, J., Tubiello, F., Chhetri, N., Dunlop, M., 2007. Adapting agriculture to climate change. *Proc. Natl. Acad. Sci. U. S. A.* 104, 19691–19696. <https://doi.org/10.1073/pnas.0701890104>.
- IPCC, 2013. *Climate Change 2013: The Physical Basis. Contribution of Working Group 1 to the Fifth Assessment Report of the IPCC*. Cambridge University Press.
- Jagai, J.S., Li, Q., Wang, S., Messier, K.P., Wade, T.J., Hilborn, E.D., 2015. Extreme precipitation and emergency room visits for gastrointestinal illness in areas with and without combined sewer systems: an analysis of Massachusetts data, 2003–2007. *Environ. Health Perspect.* 123, 873–879. <https://doi.org/10.1289/ehp.1408971>.
- Kalnay, E., Kanamitsu, M., Kistler, R., Collins, W., Deaven, D., Gandin, L., Iredell, M., Saha, S., White, G., Woollen, J., Zhu, Y., Leetmaa, A., Reynolds, R., Chelliah, M., Ebisuzaki, W., Higgins, W., Janowiak, J., Mo, K.C., Ropelewski, C., Wang, J., Jenne, R., Joseph, D., Kalnay, E., Kanamitsu, M., Kistler, R., Collins, W., Deaven, D., Gandin, L., Iredell, M., Saha, S., White, G., Woollen, J., Zhu, Y., Leetmaa, A., Reynolds, R., Chelliah, M., Ebisuzaki, W., Higgins, W., Janowiak, J., Mo, K.C., Ropelewski, C., Wang, J., Jenne, R., Joseph, D., 1996. The NCEP/NCAR 40-year reanalysis project. *Bull. Am. Meteorol. Soc.* 77, 437–471. [https://doi.org/10.1175/1520-0477\(1996\)077<0437:TNYRP>2.0.CO;2](https://doi.org/10.1175/1520-0477(1996)077<0437:TNYRP>2.0.CO;2).
- Kim, J., 2005. A projection of the effects of the climate change induced by increased CO₂ on extreme hydrologic events in the Western U.S. *Clim. Chang.* 68, 153–168. <https://doi.org/10.1007/s10584-005-4787-9>.
- Knapp, A.K., Beier, C., Briske, D.D., Classen, A.T., Luo, Y., Reichstein, M., Smith, M.D., Smith, S.D., Bell, J.E., Fay, P.A., Heisler, J.L., Leavitt, S.W., Sherry, R., Smith, B., Weng, E., 2008. Consequences of more extreme precipitation regimes for terrestrial ecosystems. *BioScience* 58, 811. <https://doi.org/10.1641/B580908>.
- Kumar, S., Lawrence, D., 2014. Less reliable water availability in the 21st century climate projections. *Earth's Futur.* 1–9. <https://doi.org/10.1002/2013EF000159>.
- Lee, S.-Y., Hamlet, A.F., Fitzgerald, C.J., Burges, S.J., 2009. Optimized flood control in the Columbia River basin for a global warming scenario. *J. Water Resour. Plan. Manag.* 135, 440–450. [https://doi.org/10.1061/\(ASCE\)0733-9496\(2009\)135:6\(440\)](https://doi.org/10.1061/(ASCE)0733-9496(2009)135:6(440)).
- Li, Z., Huang, G., Wang, X., Han, J., Fan, Y., 2016. Impacts of future climate change on river discharge based on hydrological inference: a case study of the Grand River Watershed in Ontario, Canada. *Sci. Total Environ.* 548–549, 198–210. <https://doi.org/10.1016/j.scitotenv.2016.01.002>.
- Liang, X., Lettenmaier, D.P., Wood, E.F., Burges, J., 1994. A simple hydrologically based model of land surface water and energy fluxes for general circulation models. *J. Geophys. Res.* 99, 14415–14428. <https://doi.org/10.1029/94jd00483>.
- Liang, X., Wood, E.F., Lettenmaier, D.P., 1996. Surface soil moisture parameterization of the VIC-2L model: evaluation and modification. *Global Planet. Change* 13, 195–206. [https://doi.org/10.1016/0921-8181\(95\)00046-1](https://doi.org/10.1016/0921-8181(95)00046-1).
- Livneh, B., Rosenberg, E.A., Lin, C., Nijssen, B., Mishra, V., Andreadis, K.M., Maurer, E.P., Lettenmaier, D.P., 2013. A long-term hydrologically based dataset of land surface fluxes and states for the conterminous United States: update and extensions. *J. Clim.* 26, 9384–9392. <https://doi.org/10.1175/JCLI-D-12-00508.1>.
- Lohmann, D., Rashke, E., Nijssen, B., Lettenmaier, D.P., 1998. Regional scale hydrology: I. formulation of the VIC-2L model coupled to a routing model. *Hydrol. Sci. J.* 43, 131–141. <https://doi.org/10.1080/02626669809492107>.
- Madsen, H., Lawrence, D., Lang, M., Martinkova, M., Kjeldsen, T.R., 2014. Review of trend analysis and climate change projections of extreme precipitation and floods in Europe. *J. Hydrol.* 519, 3634–3650. <https://doi.org/10.1016/j.jhydrol.2014.11.003>.
- Melsen, L.A., Addor, N., Mizukami, N., Newman, A.J., Torfs, P.J.J.F., Clark, M.P., Uijlenhoet, R., Teuling, A.J., 2018. Mapping (dis)agreement in hydrologic projections. *Hydrol. Earth Syst. Sci.* 22. <https://doi.org/10.5194/hess-22-1775-2018>.
- Mendoza, P.A., Clark, M.P., Mizukami, N., Newman, A., Barlage, M., Gutmann, E., Rasmussen, R.M., Rajagopalan, B., Brekke, L., Arnold, J.R., 2015. Effects of hydrologic model choice and calibration on the portrayal of climate change impacts. *J. Hydrometeorol.* 16 (141229151801000). <https://doi.org/10.1175/JHM-D-14-0104.1>.
- Milly, P.C.D., Wetherald, R.T., Dunne, K.A., Delworth, T.L., 2002. Increasing risk of great floods in a changing climate. *Nature* 415, 514–517. <https://doi.org/10.1038/415514a>.
- Milly, A.P.C.D., Betancourt, J., Falkenmark, M., Hirsch, R.M., Zigniew, W., Lettenmaier, D.P., Stouffer, R.J., Milly, P.C.D., 2008. Stationarity is dead: stationarity whither water management? *Science* 319, 573–574. <https://doi.org/10.1126/science.1151915>.
- Naz, B.S., Kao, S.-C., Ashfaq, M., Rastogi, D., Mei, R., Bowling, L.C., 2016. Regional hydrologic response to climate change in the conterminous United States using high-resolution hydroclimate simulations. *Glob. Planet. Change* 143, 100–117. <https://doi.org/10.1016/j.gloplacha.2016.06.003>.
- Ockenden, M.C., Deasy, C.E., Benskin, C.M.W.H., Beven, K.J., Burke, S., Collins, A.L., Evans, R., Falloon, P.D., Forber, K.J., Hiscock, K.M., Holloway, M.J., Kahana, R., Macleod, C.J.A., Reaney, S.M., Snell, M.A., Villamizar, M.L., Wearing, C., Withers, P.J.A., Zhou, J.G., Haygarth, P.M., 2016. Changing climate and nutrient transfers: evidence from high temporal resolution concentration-flow dynamics in headwater catchments. *Sci. Total Environ.* 548–549, 325–339. <https://doi.org/10.1016/j.scitotenv.2015.12.086>.
- Parnesan, C., Yohe, G., 2003. A globally coherent fingerprint of climate change impacts across natural systems. *Nature* 421, 37–42. <https://doi.org/10.1038/nature01286>.
- Parsons, M., McLoughlin, C.A., Kotschy, K.A., Rogers, K.H., Rountree, M.W., 2005. The effects of extreme floods on the biophysical heterogeneity of river landscapes. *Front. Ecol. Environ.* 3, 487–494. [https://doi.org/10.1890/1540-9295\(2005\)003\[0487:TEOEF0\]2.0.CO;2](https://doi.org/10.1890/1540-9295(2005)003[0487:TEOEF0]2.0.CO;2).
- Patz, J.A., Campbell-Lendrum, D.H., Holloway, T., Foley, J.A., 2005. *Impact of regional climate change on human health*. *Nature* 438, 310–317.
- Pryor, S., Scavia, D., Downer, C., Gaden, M., Iverson, L., Nordstrom, R., Patz, J., Roberson, G., 2014. Ch. 18: Midwest. Climate Change Impacts in the United States: The Third National Climate Assessment. pp. 418–440. <https://doi.org/10.7930/J01012N>.
- Rasmussen, R., Ikeda, K., Liu, C., Gochis, D., Clark, M., Dai, A., Gutmann, E., Dudhia, J., Chen, F., Barlage, M., Yates, D., Zhang, G., 2014. Climate change impacts on the water balance of the Colorado headwaters: high-resolution regional climate model simulations. *J. Hydrometeorol.* 15, 1091–1116. <https://doi.org/10.1175/JHM-D-13-0118.1>.
- Rosenberg, E.A., Keys, P.W., Booth, D.B., Hartley, D., Burkey, J., Steinemann, A.C., Lettenmaier, D.P., 2010. Precipitation extremes and the impacts of climate change on stormwater infrastructure in Washington State. *Clim. Chang.* 102, 319–349. <https://doi.org/10.1007/s10584-010-9847-0>.
- Schewe, J., Heinke, J., Gerten, D., Haddeland, I., Arnell, N.W., Clark, D.B., Dankers, R., Eisner, S., Fekete, B.M., Colón-González, F.J., Gosling, S.N., Kim, H., Liu, X., Masaki, Y., Portmann, F.T., Satoh, Y., Stacke, T., Tang, Q., Wada, Y., Wisser, D., Albrecht, T., Frieler, K., Piontek, F., Warszawski, L., Kabat, P., 2014. Multimodel assessment of water scarcity under climate change. *Proc. Natl. Acad. Sci. U. S. A.* 111, 3245–3250. <https://doi.org/10.1073/pnas.1222460110>.
- Schwartz, M., Hall, A., Sun, F., Walton, D., Berg, N., 2017. Significant and inevitable end-of-21 st-century advances in surface runoff timing in California's Sierra Nevada. *J. Hydrometeorol.* <https://doi.org/10.1175/JHM-D-16-0257.1>.
- Sharma, A., Hamlet, A.F., Fernando, H.J.S., Catlett, C.E., Horton, D.E., Kotamarthi, V.R., et al., 2018. The need for an integrated land-lake-atmosphere modeling system,

- exemplified by North America's Great Lakes region. *Earth's Futur.* 6. <https://doi.org/10.1029/2018EF000870>.
- Sheffield, J., Wood, E.F., 2008. Projected changes in drought occurrence under future global warming from multi-model, multi-scenario, IPCC AR4 simulations. *Clim. Dyn.* 31, 79–105. <https://doi.org/10.1007/s00382-007-0340-z>.
- Slack, J.R., Landwehr, J.M., 1992. Hydro-climatic data network (HCDN); a U.S. Geological Survey streamflow data set for the United States for the study of climate variations, 1874–1988. *Open File Rep.* 193, 92–129.
- Tohver, I.M., Hamlet, A.F., Lee, S.Y., 2014. Impacts of 21st-century climate change on hydrologic extremes in the Pacific northwest region of North America. *J. Am. Water Resour. Assoc.* 50, 1461–1476. <https://doi.org/10.1111/jawr.12199>.
- Touma, D., Ashfaq, M., Nayak, M.A., Kao, S.C., Diffenbaugh, N.S., 2015. A multi-model and multi-index evaluation of drought characteristics in the 21st century. *J. Hydrol.* 526, 196–207. <https://doi.org/10.1016/j.jhydrol.2014.12.011>.
- van Vuuren, D.P., Edmonds, J., Kainuma, M., Riahi, K., Thomson, A., Hibbard, K., Hurtt, G.C., Kram, T., Krey, V., Lamarque, J.F., Masui, T., Meinshausen, M., Nakicenovic, N., Smith, S.J., Rose, S.K., 2011. The representative concentration pathways: an overview. *Clim. Chang.* 109, 5–31. <https://doi.org/10.1007/s10584-011-0148-z>.
- Vano, J.A., Nijssen, B., Lettenmaier, D.P., 2015. Seasonal hydrologic responses to climate change in the Pacific Northwest. *Water Resour. Res.* 51, 1959–1976.
- Verma, S., Bhattarai, R., Bosch, N.S., Cooke, R.C., Kalita, P.K., Markus, M., 2015. Climate change impacts on flow, sediment and nutrient export in a Great Lakes watershed using SWAT. *Clean: Soil, Air, Water* 43, 1464–1474. <https://doi.org/10.1002/clen.201400724>.
- Vörösmarty, C.J., Vo, C.J., Green, P., 2000. Global water resources: vulnerability from climate change and population growth. *Science*, 284–288 <https://doi.org/10.1126/science.289.5477.284>.
- Wang, D., Cai, X., 2010. Comparative study of climate and human impacts on seasonal baseflow in urban and agricultural watersheds. *Geophys. Res. Lett.* 37. <https://doi.org/10.1029/2009GL041879>.
- Wang, X., Huang, G., Liu, J., 2014. Projected increases in intensity and frequency of rainfall extremes through a regional climate modeling approach. *J. Geophys. Res.-Atmos.*, 271–286 <https://doi.org/10.1002/2014JD022564>.
- Wang, X., Huang, G., Liu, J., Li, Z., Zhao, S., 2015. Ensemble projections of regional climatic changes over Ontario, Canada. *J. Clim.* 28, 7327–7346. <https://doi.org/10.1175/JCLI-D-15-0185.1>.
- Wenger, S.J., Isaak, D.J., Luce, C.H., Neville, H.M., Fausch, K.D., Dunham, J.B., Dauwalter, D.C., Young, M.K., Elsner, M.M., Rieman, B.E., Hamlet, A.F., Williams, J.E., 2011. Flow regime, temperature, and biotic interactions drive differential declines of trout species under climate change. *Proc. Natl. Acad. Sci. U. S. A.* 108, 14175–14180. <https://doi.org/10.1073/pnas.1103097108>.
- Wheeler, T., von Braun, J., 2013. Climate change impacts on global food security. *Science* 341, 508–513. <https://doi.org/10.1126/science.1239402>.
- Wilby, R.L., Troni, J., Biot, Y., Tedd, L., Hewitson, B.C., Smith, D.M., Sutton, R.T., 2009. A review of climate risk information for adaptation and development planning. *Int. J. Climatol.* 29, 1193–1215. <https://doi.org/10.1002/joc.1839>.
- Wong, C.P., Jiang, B., Kinzig, A.P., Lee, K.N., Ouyang, Z., 2015. Linking ecosystem characteristics to final ecosystem services for public policy. *Ecol. Lett.* 18, 108–118. <https://doi.org/10.1111/ele.12389>.
- Wood, A.W., Leung, L.R., Sridhar, V., Lettenmaier, D.P., 2004. Hydrologic implications of dynamical and statistical approaches to downscaling climate model outputs. *Clim. Chang.* 62, 189–216. <https://doi.org/10.1023/B:CLIM.0000013685.99609.9e>.
- Zhou, Q., Mikkelsen, P.S., Halsnaes, K., Arnbjerg-Nielsen, K., 2012. Framework for economic pluvial flood risk assessment considering climate change effects and adaptation benefits. *J. Hydrol.* 414–415, 539–549. <https://doi.org/10.1016/j.jhydrol.2011.11.031>.